Open access • Posted Content • DOI:10.1101/2020.05.08.084749

Condensation of pericentrin proteins in human cells illuminates phase separation in centrosome assembly — Source link

Xueer Jiang, Dac Bang Tam Ho, Karan Mahe, Jennielee Mia ...+4 more authors

Institutions: University of California, Davis, University of California, Berkeley

Published on: 10 May 2020 - bioRxiv (Cold Spring Harbor Laboratory)

Topics: Pericentriolar material, PCNT, Centrosome, Centriole and Mitosis

Condensation of pericentrin proteins in human cells illuminates phase separation in centrosome assembly

Xueer Jiang[1], Dac Bang Tam Ho[1], Karan Mahe[1], Jennielee Mia[1], Guadalupe Sepulveda[1†], Mark Antkowiak[1‖], Soichiro Yamada[2], and Li-En Jao[1*]

Affiliations

[1]Department of Cell Biology and Human Anatomy, University of California, Davis, School of Medicine, Davis, CA 95616, USA

[2]Department of Biomedical Engineering, University of California, Davis, Davis, CA 95616, USA

[†]Current address: Department of Molecular and Cell Biology, University of California, Berkeley, Berkeley, CA 94720, USA

[‖]Current address: Northwestern University, Feinberg School of Medicine, Chicago, IL 60611, USA

[*]For correspondence: ljao@ucdavis.edu

Abstract

Mitotic centrosomes are complex membraneless organelles that guide the formation of mitotic spindles to ensure faithful cell division. They are formed by timely expansion of the pericentriolar material (PCM) around the centrioles at the onset of mitosis. How PCM proteins are recruited and held together without a lipid membrane remains elusive. Here we found that endogenously expressed pericentrin (PCNT), a conserved PCM scaffold protein, condenses into liquid-like granules during early mitosis in cultured human cells. Furthermore, the N-terminal segment of PCNT, enriched with conserved coiled-coils and low-complexity regions (LCRs), undergoes phase separation. These PCNT “condensates” selectively recruit PCM components and nucleate microtubules in cells. We propose that coiled-coils and LCRs, two prevalent sequence features in the centrosomal proteome, are preserved under evolutionary pressure to drive phase separation, a process that bestows upon the centrosome a distinct material property critical for its assembly and functions.

Introduction

The centrosome serves as a major microtubule-organizing center (MTOC) in animal cells. It consists of a pair of centrioles embedded in a proteinaceous network of pericentriolar material (PCM) (Conduit et al., 2015; Rieder & Borisy, 1982; Vorobjev & Chentsov Yu, 1982; Wang et al., 2011; Woodruff et al., 2014). The MTOC activity of the centrosome is determined by the PCM, which acts as a scaffold to recruit MT regulators and nucleators, such as γ-tubulin ring complexes (γ-TuRCs) (Jeng & Stearns, 1999; Moritz, Braunfeld, Sedat, et al., 1995; Moritz et al., 1998; Oegema et al., 1999; Zheng et al., 1995). The PCM is not a static structure. In interphase cells, relatively small amounts of PCM are assembled around the centriole and organized as a layered, nanometer-sized toroid (Fu & Glover, 2012; Lawo et al., 2012; Mennella et al., 2012; Sonnen et al., 2012). As the cell enters mitosis, the PCM expands dramatically into a micron-sized ensemble, with a concomitant increase in its MTOC activity as the mitotic spindle forms in a process termed centrosome maturation (Mahen & Venkitaraman, 2012; Mennella et al., 2014; Palazzo et al., 2000).

Over the past decades, proteins important for centrosome maturation have been identified (Andersen et al., 2003; Dobbelaere et al., 2008; Goshima et al., 2007; Hamill et al., 2002; Hutchins et al., 2010; Neumann et al., 2010; Sonnichsen et al., 2005; Woodruff et al., 2015). At the molecular level, centrosome maturation is initiated upon phosphorylation of core PCM components, such as spindle-defective protein 5 (SPD-5), centrosomin (Cnn), and pericentrin (PCNT) by mitotic kinases Polo/PLK1 and aurora kinase A (Barr & Gergely, 2007; Berdnik & Knoblich, 2002; Conduit, Feng, et al., 2014; Hannak et al., 2001; Joukov et al., 2014; Kinoshita et al., 2005; Lee & Rhee, 2011; Woodruff et al., 2017; Woodruff et al., 2015; Wueseke et al., 2016). This triggers the cooperative assembly of additional PCM proteins (Alvarez-Rodrigo et al., 2019; Conduit, Richens, et al., 2014; Hamill et al., 2002; Kemp et al., 2004; Meng et al.,

2015) and γ-TuRCs to facilitate bipolar spindle assembly (Conduit et al., 2015; Jeng & Stearns, 1999; Khodjakov & Rieder, 1999; Moritz, Braunfeld, Sedat, et al., 1995; Moritz et al., 1998; Oegema et al., 1999; Piehl et al., 2004; Woodruff et al., 2014; Zheng et al., 1995). While the mechanism of centrosome maturation has been elucidated at the molecular level, the biophysical principle of PCM assembly remains elusive at the organellar level—without an enclosing membrane, what keeps the crowded PCM proteins from dispersing?

Liquid-liquid phase separation, a process through which macromolecules de-mix and partition from a single phase into two or more distinct phases in a concentration-dependent manner, has emerged as a mechanism that underlies a variety of cellular processes involving non-membrane-bound compartments or organelles (reviews in Banani et al., 2017; Holehouse & Pappu, 2018; Hyman et al., 2014; Shin & Brangwynne, 2017). Recently Woodruff and colleagues proposed that the centrosome is formed through phase separation (Woodruff et al., 2017). They showed that *in vitro* purified SPD-5, a core PCM protein with extensive coiled-coils in *C. elegans* (Hamill et al., 2002), forms spherical liquid "condensates" *in vitro* in the presence of crowding reagents, which mimic the dense cytoplasm (Woodruff et al., 2017). SPD-5 condensates possess a centrosomal activity *in vitro*, capable of nucleating MTs after selectively recruiting tubulin dimers and cognate proteins (ZYG-9 and TPXL-1) (Woodruff et al., 2017). These data are also consistent with mathematical modeling of centrosomes as autocatalytic droplets formed by phase separation (Zwicker et al., 2014). However, it is unclear how closely this *in vitro* system actually reflects centrosomal MT nucleation *in vivo*, as SPD-5 condensates do not recruit γ-tubulin, an essential *in vivo* MT nucleation factor for many species (Felix et al., 1994; Hannak et al., 2002; Joshi et al., 1992; Oakley et al., 1990; Stearns et al., 1991; Stearns & Kirschner, 1994; Zheng et al., 1991).

Contrary data suggest that phase separation may not play a role in centrosome assembly. For example, Cnn—a major mitotic PCM component and functional homolog of SPD-5 in

Drosophila—does not undergo dynamic internal rearrangements as it incorporates into the centrosome *in vivo* (Conduit et al., 2010; Conduit, Feng, et al., 2014). Two short conserved domains of Cnn can self-assemble into solid-like scaffolds *in vitro*, but no liquid-to-solid phase transition has been observed (Feng et al., 2017). However, the action of these Cnn segments in the context of full-length Cnn *in vivo* remains unknown. Together, with the available evidence, it remains elusive whether liquid-liquid phase separation underlies centrosome assembly.

In vertebrates, PCNT plays a particularly important role in PCM assembly as it is required for the initiation (Lee & Rhee, 2011; Zimmerman et al., 2004) and recruitment of key PCM components during centrosome maturation (Haren et al., 2009; Lawo et al., 2012; Zimmerman et al., 2004). We recently showed that PCNT enrichment during centrosome maturation is controlled by a co-translational targeting mechanism that ensures timely production and spatial deposition of PCNT at the centrosome (Sepulveda et al., 2018). Indeed, PCNT expression is tightly regulated. For example, human loss-of-function mutations of PCNT cause microcephalic osteodysplastic primordial dwarfism type II (Anitha et al., 2009; Delaval & Doxsey, 2010; Griffith et al., 2008; Numata et al., 2009; Rauch et al., 2008), whereas elevated PCNT levels disrupt ciliary protein trafficking and sonic hedgehog signaling, and may contribute to clinical features of Down syndrome (Galati et al., 2018). Despite its importance at the cellular and organismal levels, the precise function of PCNT in centrosome assembly remains enigmatic.

Here we demonstrate that endogenously GFP-tagged human PCNT forms droplet-like pericentrosomal granules during early mitosis. These GFP-PCNT granules show liquid-like properties as they fuse and split in seconds and are dissolved by hexanediol that disrupts weak protein-protein interactions. These data suggest that PCNT phase separates into liquid-like condensates at physiologically relevant levels during mitosis. We further show that phase separation of PCNT is driven by the segments enriched with conserved coiled-coils and low-complexity regions (LCRs). These PCNT condensates transition from liquid- to gel/solid-like

107 states and exhibit centrosome-like activities in cells, including selectively recruiting endogenous
108 PCM components and nucleating MTs. The finding that PCNT undergoes liquid-liquid phase
109 separation under physiologically relevant conditions provides insights into the role of coiled-coils
110 and LCRs in the assembly of the membraneless centrosome, which is enriched with proteins
111 containing both sequence features.

Results

Endogenously expressed GFP-PCNT forms liquid-like condensates during early mitosis

To test whether PCNT undergoes liquid-liquid phase separation under physiologically relevant conditions in mammalian cells, we generated stable human cell lines with GFP-tagged PCNT expressed from its endogenous locus using the CRISPR technology (S. Lin et al., 2014; Zhang et al., 2017). We inserted a super-folder GFP (sfGFP) cassette at the 5' end (exon 1) of the *PCNT* allele in hTERT-immortalized human retinal pigment epithelial cells (RPE-1 cells) (**Figure 1- figure supplement 1**). The resulting knock-in cell lines exhibited normal cell morphology and mitotic progression with the GFP-PCNT decorating the centrosomes as expected (**Figure 1- figure supplement 1**).

Through high-resolution time-lapse confocal microscopy, we observed small GFP-PCNT granules (100-400 nm) near centrosomes in early mitosis (**Figure 1A and Figure 1- movie supplement 1 and 2**). Similar pericentrosomal PCNT granules were also observed by immunostaining endogenous, untagged PCNT during early mitosis (Sepulveda et al., 2018) (**Figure 1- figure supplement 2**). These GFP-PCNT granules were dynamic and appeared to fuse and split over a timescale of seconds. Similar dynamic pericentrosomal GFP-PCNT granules were also observed in another independent knock-in clone (**Figure 1- movie supplement 3**). This dynamic behavior suggests that these PCNT granules may be liquid-like condensates formed by liquid-liquid phase separation. To test this hypothesis, we treated the cells with aliphatic alcohol 1,6-hexanediol, which dissolves liquid-like condensates by disrupting weak hydrophobic interactions (Kroschwald et al., 2017; Ribbeck & Gorlich, 2002). Following hexanediol addition, PCNT granules near centrosomes dispersed within minutes (**Figure 1B and C**). Together, these results suggest that PCNT, expressed from its endogenous locus,

forms liquid-like condensates, likely through liquid-liquid phase separation, before incorporating into the early mitotic centrosome of cultured human cells.

Coiled-coils and low-complexity regions of pericentrin are more conserved than the rest of the protein sequence

If condensation of PCNT is of evolutionary significance, the sequence features that contribute to condensation should be conserved across species and may be identifiable at the primary sequence level. To test this hypothesis, we constructed an alignment of 169 pericentrin orthologous proteins—167 from vertebrates, one from fruit fly (D-PLP, Martinez-Campos et al., 2004), and one from budding yeast (Spc110, Knop & Schiebel, 1997; Sundberg & Davis, 1997) (**Figure 2A and Figure 2- table 1**). A number of sequence blocks are highly conserved. A prominent one is located at the C-terminus, particularly at the PACT motif, a hallmark pericentrin domain known for centrosomal anchoring (Gillingham & Munro, 2000; Takahashi et al., 2002). Another highly conserved region is in the middle portion of the protein. In contrast, the N-terminus is not well conserved, with the evidence of clade-specific insertions.

To gain insights into the properties of these conserved sequences, we performed further *in silico* analyses (Lupas et al., 1991; Wootton, 1994), focusing on human PCNT. We found that similar to other centrosomal proteins, human PCNT is enriched with coiled-coils and low-complexity regions (LCRs) (**Figure 2A**). LCRs often overlap with intrinsically disordered regions, which can mediate multivalent interactions to drive or tune liquid-liquid phase separation (Boke et al., 2016; Kato et al., 2012; Lin et al., 2015; Molliex et al., 2015; Patel et al., 2015; Riback et al., 2017). Indeed some disorder predictors (e.g., PONDR, Peng et al., 2006; Peng et al., 2005) predicted that human PCNT is largely disordered except for the C-terminal PACT motif (**Figure 2- figure supplement 1**). However, as a known limitation with current disorder predictions

(Atkins et al., 2015), not all disorder predictors are in complete agreement, with each predictor suggesting different degrees of disorder/order tendency [e.g., IUpred (Dosztanyi et al., 2005) predicted an overall more ordered structure than PONDR did].

Nonetheless, by comparing the conservation profile of the multi-species alignment and the locations of the predicted features of human PCNT, we found that the coiled-coils and LCRs in human PCNT are concentrated within the conserved orthologous regions (**Figure 2A**). Statistical analyses further demonstrated that coiled-coils and LCRs are significantly more conserved than non-coiled-coils and non-LCRs, respectively, in human PCNT (**Figure 2B**). Together, these results suggest that coiled-coils and LCRs of pericentrin orthologs are likely under natural selection to preserve their molecular functions.

PCNT phase separates via its coiled-coil/LCR-rich segments in a concentration-dependent manner

Given that both coiled-coils and LCRs can drive liquid-liquid phase separation (Berry et al., 2015; Boeynaems et al., 2018; Elbaum-Garfinkle et al., 2015; Fang et al., 2019; Hennig et al., 2015; Lu et al., 2020; Molliex et al., 2015; Nott et al., 2015; Smith et al., 2016; Wang et al., 2018; Wippich et al., 2013; Zeng et al., 2016; Zhang et al., 2018), we hypothesized that the coiled-coil/LCR-rich sequences drive phase separation of the full-length PCNT observed in the knock-in cells.

To test this hypothesis, control PCNT transcription tightly, and map phase separation determinants, we divided PCNT into N- and C-terminal segments, tagged each with sfGFP, and subcloned the resulting GFP-PCNT constructs under the control of a doxycycline (Dox)-inducible promoter. We then stably integrated each construct in RPE-1 cells using a *piggyBac* transposon system (Kim et al., 2016). Upon Dox induction, live cell imaging showed that the N-

terminal segment, GFP-PCNT (2-1960), formed dynamic condensates (**Figure 2C and Figure 2- movie supplement 1**) with fast internal rearrangement of molecules ($t_{1/2}$ = 260 ms) as determined by fluorescence recovery after photobleaching (FRAP) assays (**Figure 2D**). In contrast, the C-terminal segment, GFP-PCNT (1954-3336), formed solid-like scaffolds (**Figure 2C and Figure 2- movie supplement 2**) with little internal rearrangement or fluorescence recovery (**Figure 2D**).

To further map the phase separation driver sequences, we tested GFP-tagged PCNT (2-891) and (854-1960) constructs, which subdivide PCNT (2-1960) but do not disrupt predicted individual coiled-coils or LCRs. After inducing their expression in cells, we compared their respective critical concentrations, the point above which liquid-liquid phase separation occurs (Asherie, 2004). To quantitatively assess this value in living cells, we developed an imaging and quantification workflow to measure relative protein concentrations by fluorescence intensity per voxel (volume). With this workflow, we found that GFP-PCNT (2-891) remained diffuse in cells as its concentration increased. However, over the same concentration range, GFP-PCNT (854-1960) suddenly formed droplet-like condensates when it reached its critical concentration for phase separation (**Figure 2E,** also see **Figure 3**). Using this workflow, we also validated the liquid-liquid phase separation behavior of GFP-PCNT (2-1960)—which had a slightly higher critical concentration than GFP-PCNT (854-1960)—and the lack of phase separation for GFP-PCNT (1954-3336) within the same concentration range (**Figure 2E**). Collectively, these results suggest that the abundant coiled-coils and LCRs between residues 854 and 1960 of human PCNT—which are also well conserved across species (**Figure 2A and B**)—contain the key sequence elements that mediate PCNT phase separation.

205 **GFP-PCNT (854-1960) undergoes liquid-liquid phase separation, coalesces, and moves**
206 **toward the centrosome**

207 Besides phase separating at a lower concentration than GFP-PCNT (2-1960) (**Figure 2E**),
208 GFP-PCNT (854-1960) condensates also exhibited different morphology and behavior. In
209 particular, early-stage small GFP-PCNT (854-1960) condensates formed well-defined spherical,
210 liquid-like droplets as they rapidly split and fused within seconds (**Figure 3A**). Over time, these
211 GFP-PCNT (854-1960) condensates coalesced and converged at the centrosome—arcing
212 around the nucleus in some cases—to form large pericentrosomal blobs (**Figure 3B and Figure**
213 **3- movie supplement 1**). Their movement is likely mediated by dynein motors as this PCNT
214 segment contains a putative dynein-binding domain (Tynan et al., 2000) (**Figure 2A**).
215 Importantly, since FLAG- and mScarlet-i-tagged PCNT (854-1960) fusion proteins also formed
216 similar condensates (**Figure 3- figure supplement 1 and Figure 3- movie supplement 2**), the
217 GFP tag did not artifactually drive liquid-liquid phase separation.

218 Close examination of time-lapse data revealed that the rate of fusing and splitting decreased
219 as PCNT (854-1960) condensates coalesced (**Figure 3B and Figure 3- movie supplement 1**
220 **and 2**), suggesting that the viscosity of PCNT (854-1960) condensates increased over time. To
221 test this hypothesis, we used the Dox-inducible system to induce, track, and analyze material
222 properties of young (0-3 h old) and old (20-24 h old) GFP-PCNT (854-1960) condensates by
223 FRAP. We found that young condensates recovered fluorescence almost twice as fast as the
224 old ones (**Figure 3C**). Some young condensates recovered >100% of their initial fluorescence
225 intensity because they grew in size. These results suggest that GFP-PCNT (854-1960)
226 condensates become “hardened” over time. Such molecular aging is also reported for other
227 proteins that phase separate *in vitro*, such as SPD-5 (Woodruff et al., 2017), FUS (Patel et al.,
228 2015), hnRNPA1 (Lin et al., 2015), and Tau (Wegmann et al., 2018).

GFP-PCNT (854-1960) condensates selectively recruit endogenous PCM components

Because the "hardened" SPD-5 condensates recruit tubulins and factors involved in MT nucleation *in vitro* (Woodruff et al., 2017), we tested whether GFP-PCNT (854-1960) condensates can also recruit PCM components, including structural polypeptides and "client" proteins, which are also recruited to mitotic PCM (e.g., dynein and PLK1). We found that endogenous PCNT, γ-tubulin, CEP215, CEP192, dynein intermediate chains (ICs), and PLK1 were significantly enriched in GFP-PCNT (854-1960) condensates, whereas the non-PCM component ribosomal protein S6 (RPS6) was excluded (**Figure 4**). Interestingly, these recruited proteins were nonuniformly distributed, with reticular patterns that resemble mitotic PCM (Lawo et al., 2012; Sonnen et al., 2012). To exclude the possibility that any phase-separated condensates could recruit PCM components, we examined the enrichment of PCM components in the condensates formed by HOTags, the *de novo*-designed homo-oligomeric coiled-coils (Grigoryan et al., 2011; Huang et al., 2014; Thomson et al., 2014), which phase separate through multivalent interactions (Zhang et al., 2018). We found that PCM components γ-tubulin, PCNT, and CEP192 were not enriched in the HOTag condensates (**Figure 4- figure supplement 1**). Collectively, these results indicate that PCNT (854-1960) condensates possess a unique material property that enables them to selectively recruit endogenous PCM components.

GFP-PCNT (854-1960) condensates nucleate microtubules in cells

Since PCNT (854-1960) condensates recruit γ-tubulin (**Figure 4**), the protein that plays a central role in MT nucleation (Felix et al., 1994; Hannak et al., 2002; Joshi et al., 1992; Oakley et al., 1990; Stearns et al., 1991; Stearns & Kirschner, 1994; Zheng et al., 1991), we tested whether these condensates can also nucleate MTs in cells by performing a MT renucleation

assay (Jao et al., 2017; Sanders et al., 2017). In this assay, we treated cells with nocodazole to depolymerize MTs, washed out the drug, and monitored renucleation of MTs by anti-α-tubulin immunostaining. We found that MTs were renucleated not only from the centrosome as expected, but also from the interior and surface of PCNT condensates (**Figure 5A, arrows**). The condensates also recruited endogenous PCNT as observed before. Some small PCNT condensates also recruited endogenous PCNT and nucleated MTs (**Figure 5B, inlets, asterisks**). Quantification of MT density in condensates and their surrounding cytoplasm confirmed that PCNT condensates have a significantly higher MT renucleation activity than the surrounding cytoplasm (**Figure 5C**). A similar MT renucleation assay was also performed in live cells, where EB3-tdTomato was used to track the growing MT plus ends. Live cell imaging showed that some PCNT condensates nucleated MTs as EB3-tdTomato signals were emanating from the surface of the PCNT condensates (**Figure 5- figure supplement 1**). From these two MT renucleation assays, we conclude that GFP-PCNT (854-1960) condensates possess the centrosome-like MT nucleation activity in cells.

Discussion

Our work shows that endogenously expressed PCNT, a core PCM protein important for centrosome maturation, forms liquid-like granules before incorporating into mitotic centrosomes in human cells. These PCNT granules are likely formed through liquid-liquid phase separation because (1) they are sensitive to the acute hexanediol treatment that is known to disrupt phase-separated condensates (Kroschwald et al., 2017; Larson et al., 2017; So et al., 2019; Strom et al., 2017) and (2) the coiled-coil/LCR-rich portion of PCNT undergoes concentration-dependent condensation *in cellulo* that obeys characteristics of phase separation, including a sharp phase transition boundary, condensate coalescence, deformability, and fast recovery in FRAP experiments. Recent theoretical modeling (Zwicker et al., 2014) and *in vitro* reconstitution studies (Woodruff et al., 2017) suggest that liquid-liquid phase separation underlies centrosome assembly in *C. elegans*. To our knowledge, our study provides the first *in cellulo* evidence to support such a model and suggests that phase separation may also underlie the assembly of vertebrate centrosomes with at least one protein, PCNT, directly involved in this process.

Is co-translational targeting of PCNT linked to its condensation during early mitosis?

The liquid-like PCNT granules are predominantly observed during early mitosis when co-translational targeting of PCNT to the centrosome peaks (Sepulveda et al., 2018). This raises an intriguing question of whether co-translational targeting facilitates PCNT phase separation. In the co-translational targeting model, multiple nascent PCNT polypeptides emerge from each polysome complex with a single large *PCNT* mRNA and are transported along the MT tracks. This process could effectively bring multiple N-terminal, phase separation-driving PCNT polypeptides in close proximity. A proximity-driven phase separation can thus be envisioned since phase separation is a concentration-dependent process. This also explains why these

liquid-like PCNT granules are observed predominantly during early mitosis when PCNT production is maximized. This proximity-driven phase separation model is also consistent with the results that phase separation of the N-terminal (2-1960) or middle (854-1960) segment of PCNT can be recapitulated in the cytoplasm in a concentration-dependent manner, when it was expressed exogenously and has reached its critical concentration.

Functional significance of liquid-like PCNT granules

What is the functional significance of PCNT condensation? Would it facilitate the centrosomal targeting and incorporation of PCNT? Or more broadly, is the formation of liquid-like PCNT granules a prerequisite for proper centrosome assembly? Woodruff and colleagues show that in the presence of crowding reagents, purified centrosomal protein SPD-5 forms liquid-like spherical condensates *in vitro*, which then rapidly "mature" into a gel- or solid-like state (Woodruff et al., 2017). Strikingly, only these spherical SPD-5 condensates can nucleate MTs, but not the solid-like SPD-5 scaffolds formed in the absence of crowding reagents (Woodruff et al., 2017; Woodruff et al., 2015). Their data thus suggest that formation of a condensate with liquid-like properties, even only transiently, might be important to allow centrosomal proteins to be properly assembled to organize MTs (Raff, 2019; Woodruff et al., 2017). A similar scenario could happen here; the formation of liquid-like PCNT granules may enable the proper assembly of the human centrosome to organize MTs, for example, by allowing various PCM components to "morph" into the desired configuration (also see below). Important future studies are to investigate whether other PCM components are co-condensed with PCNT granules, and to rationally design phase separation-deficient (and -rescuing) PCNT variants to determine the significance of phase separation *per se* in centrosome function under physiologically relevant conditions.

315 **Is there a liquid-to-gel/solid-like transition in PCM assembly?**

316 PCNT (854-1960) condensates transition from liquid- to gel/solid-like state, resulting in a
317 scaffold with an inhomogeneous, porous appearance (**Figures 3 and 4**). Morphologically, this
318 pattern resembles that of salt-stripped mitotic centrosomes purified from flies and clams in early
319 electron tomography studies (Moritz, Braunfeld, Fung, et al., 1995; Schnackenberg et al., 1998),
320 in which the PCM is shown as a fibrous, solid-like scaffold surrounding the centrioles. Moritz
321 and colleagues further demonstrate that upon adding bovine or fly tubulins, MTs regrow from
322 the PCM of the salt-stripped centrosomes, with MT nucleation sites distributed throughout the
323 PCM and MTs oriented in different directions (Moritz, Braunfeld, Fung, et al., 1995).
324 Interestingly, in our MT renucleation assays, we also observed a similar MT renucleation pattern
325 in the PCNT condensate; MTs were nucleated throughout the condensate and regrown into
326 different directions (**Figure 5 and Figure 5- figure supplement 1**). We thus speculate that
327 without the C-terminal PACT motif for centrosomal anchoring, the PCNT (854-1960) condensate
328 is allowed to grow freely in the cytoplasm (through the process of liquid-liquid phase
329 separation), eventually becoming a giant ensemble that shares a similar internal organization
330 with the real PCM. The similarity in organization between PCNT condensates and purified PCM
331 scaffolds implicates that centrosome assembly may be guided by a similar underlying principle,
332 pivoting on liquid-to-gel/solid-like phase transition.

333 What could be the advantage of assembling the centrosome through a liquid-to-gel/solid-like
334 transition? We speculate that with the liquid-like state (even just transiently), large scaffold
335 proteins such as PCNT, along with other PCM components, are allowed to establish the
336 interconnection before transitioning into the mature, gel/solid-like state. This “extra transitioning
337 step” might be particularly important in forming large, micron-sized, membraneless structures
338 such as the PCM.

How is PCNT (854-1960) capable of recruiting endogenous PCM components and nucleating MTs?

It is surprising that the PCNT condensates formed by one-third of PCNT (residues 854-1960) can selectively recruit endogenous centrosomal proteins and nucleate MTs *in cellulo*. This region is particularly enriched with coiled-coils and LCRs (**Figure 2A**) and appears to contain the sequence elements that drive phase separation. However, this region does not contain the putative γ-tubulin-binding domains, which are within the first 350 amino acids of human PCNT (T. C. Lin et al., 2014) (**Figure 2A**), nor the CEP215-binding domain, which is mapped to the C-terminus of human PCNT (amino acids 2390-2406) (Kim & Rhee, 2014). Yet both γ-tubulin and CEP215 (and several other PCM proteins) are recruited to these condensates (**Figure 4**). One explanation is that their recruitments are mediated through the endogenous PCNT that is also recruited to the condensate. Another possibility is that PCNT (854-1960) contains yet to be identified binding sites for these PCM components. It is also possible that PCNT (854-1960) condensates gain new material properties that enable selective recruitment by generating a binding environment specific for PCM components. In the future, studying the PCNT (854-1960) condensates in the *PCNT* knockout cells and reconstituting PCNT (854-1960) condensates *in vitro* to test their capability of recruiting PCM components would help distinguish these possibilities.

Re-evaluating the role of coiled-coils in centrosome assembly

Coiled-coils are often enriched with low-complexity sequences (Romero et al., 1999). They are frequently predicted to be disordered as monomers but become folded upon formation of quaternary structures (coupled folding and binding) (Anurag et al., 2012; Szappanos et al., 2010; Uversky et al., 2000). Due to these unique properties, coiled-coils are known to adapt

363 vast structural variations with different superhelical stabilities to exert a wide range of biological
364 functions (Grigoryan & Keating, 2008; Li et al., 2003; Rose & Meier, 2004).

365 It has long been recognized that coiled-coil proteins are enriched at the centrosome and
366 function as parts of the "centromatrix" for the recruitment of other proteins (Doxsey, 2001;
367 Salisbury, 2003; Schnackenberg & Palazzo, 1999). Recent *in vitro* reconstitution studies of the
368 coiled-coil PCM proteins SPD-5 (*C. elegans*) and Cnn (*Drosophila*) provide strong evidence to
369 support a polymer-based mechanism of PCM assembly (Feng et al., 2017; Woodruff et al.,
370 2017; Woodruff et al., 2015). However, the exact mechanism underlying this polymer-based
371 assembly is still under debate. It also remains unclear whether this model is applicable to
372 vertebrate systems (Gupta & Pelletier, 2017; Raff, 2019).

373 We found that in cultured human cells, not only endogenously expressed full-length human
374 PCNT condense into liquid-like granules, the coiled-coil-rich PCNT segments alone can also
375 phase separate to form bioactive condensates with centrosome-like activities. These findings
376 illuminate the fundamental principle of centrosome assembly and join a growing list of studies in
377 which coiled-coil-mediated phase separation participates in a variety of biological functions
378 (Fang et al., 2019; Lu et al., 2020; Vega et al., 2019; Zeng et al., 2016).

379 Importantly, coiled-coils and LCRs of human PCNT are enriched in the regions that are
380 evolutionarily conserved, suggesting that these sequence features are under natural selection to
381 preserve critical functions. We propose that PCNT is a linear multivalent protein that phase
382 separates through its conserved coiled-coils and LCRs to become spatially organized
383 condensates that scaffold PCM assembly. This process is likely initiated during its co-
384 translational targeting to the centrosome when the nascent PCNT polypeptides are in close
385 proximity in the polysome (**Figure 6**). We propose that PCNT phase separation achieves two
386 main goals. First, it concentrates PCM components and clients as the PCNT condensates
387 selectively recruit them. This will facilitate and limit the biochemical reactions that eventually

take place at the centrosome (e.g., MT nucleation, kinase activities). Second, it enables a liquid-to-gel/solid-like transitioning process during centrosome assembly. This process provides the PCM components a thermodynamically favored pathway to assemble into a micron-sized, membraneless, and yet spatially organized PCM.

Although coiled-coils mediate other phase separation-independent activities, it is tempting to speculate that coiled-coil-mediated phase separation might be widespread among other coiled-coil-rich centrosomal proteins as previously suggested (Woodruff et al., 2017). Our results encourage future studies to rethink the conceptional framework regarding coiled-coil proteins and phase separation in centrosome assembly and to determine whether a unified mechanism is applied across metazoans.

Materials and Methods

Key resources table

Reagent type	Reagent	Source	Cat. No	Additional information
Chemical compound, drug	1,6-Hexanediol	Sigma-Aldrich, St. Louis, MO	240117	
Chemical compound, drug	DAPI	Sigma-Aldrich, St. Louis, MO	D9542	
Chemical compound, drug	Doxycycline hyclate	Sigma-Aldrich, St. Louis, MO	D9891	
Chemical compound, drug	G418 disulfate salt	Sigma-Aldrich, St. Louis, MO	A1720	
Chemical compound, drug	Nocodazole	Sigma-Aldrich, St. Louis, MO	M1404	
Chemical compound, drug	Polybrene	Santa Cruz Biotechnology Inc., Santa Cruz, CA	SC-134220	
Chemical compound, drug	Rapamycin	LC Laboratories, Woburn, MA	R-5000	
Chemical compound, drug	RO-3306	R and D Systems, Minneapolis, MN	4181	
Chemical compound, drug	Taxol	TOCRIS Bio-Techne Corporation Minneapolis, MN	1097	
Antibody	Alexa Fluor 568 goat anti-mouse IgG [H+L]	Invitrogen, Carlsbad, CA	Invitrogen Cat# A11031, RRID: AB_144696	1:500 dilution
Antibody	Alexa Fluor 568 goat anti-rabbit IgG [H+L]	Invitrogen, Carlsbad, CA	Invitrogen Cat# A11011,	1:500 dilution

			RRID: AB_143157	
Antibody	Alexa Fluor 647 goat anti-mouse IgG [H+L]	Invitrogen, Carlsbad, CA	Invitrogen Cat# A21236, RRID: AB_2535805	1:500 dilution
Antibody	Alexa Fluor 647 goat anti-rabbit IgG [H+L]	Invitrogen, Carlsbad, CA	Invitrogen Cat# A21245, RRID: AB_2535813	1:500 dilution
Antibody	Mouse anti-alpha-tubulin	Developmental Studies Hybridoma Bank (DSHB), University of Iowa, Iowa City, IA	DSHB Cat# 12G10, RRID: AB_1157911	1:100 dilution
Antibody	Mouse anti-Dynein, 74 kDa intermediate chains, cytoplasmic, clone 74.1	EMD Millipore, Burlington, MA	EMD Millipore Cat# MAB1618, RRID: AB_2246059	1:500 dilution
Antibody	Mouse anti-hGAPDH	Developmental Studies Hybridoma Bank (DSHB), University of Iowa, Iowa City, IA	DSHB Cat# DSHB-hGAPDH-2G7, RRID: AB_2617426	1:300 dilution
Antibody	Mouse anti-PLK1	EMD Millipore, Burlington, MA	EMD Millipore Cat# 05-844, RRID: AB_310836	1:1000 dilution
Antibody	Mouse anti-p53	Abcam, Cambridge, MA	Abcam Cat# ab1101, RRID: AB_297667	1:1000 dilution
Antibody	Mouse anti-ribosomal protein S6 (C-8)	Santa Cruz Biotechnology Inc., Santa Cruz, CA	Santa Cruz Biotechnology Cat# sc-74459, RRID: AB_1129205	1:50 dilution
Antibody	Mouse anti-γ-tubulin	Sigma-Aldrich, St. Louis, MO	Sigma-Aldrich Cat# T6557, RRID: AB_477584	1:500 dilution

Antibody	Rabbit anti-CDK5RAP2 (CEP215)	EMD Millipore, Burlington, MA	EMD Millipore Cat# 06-1398, RRID: AB_11203651	1:500 dilution
Antibody	Rabbit anti-CEP192	Bethyl, Montgomery, TX	Bethyl Cat# A302-324A, RRID: AB_1850234	1:500 dilution
Antibody	Rabbit anti-PCNT N terminus	Abcam, Cambridge, MA	Abcam Cat# ab4448, RRID: AB_304461	1:1000 dilution
Commercial system or kit	Corning® 50 mL Tube Top Vacuum Filter System, 0.22 μm Pore 13.6cm² CA Membrane	Corning Inc., Corning, NY	Corning Cat# 430320	
Commercial system or kit	Lipofectamine™ 3000 Transfection Reagent	Invitrogen, Carlsbad, CA	Invitrogen Cat# L3000-008	
Commercial system or kit	Neon™ Transfection System	Invitrogen, Carlsbad, CA	MPK5000	
Commercial system or kit	Neon™ Transfection System 10 μL Kit	Invitrogen, Carlsbad, CA	MPK1096	
Cell line	HEK293T cells	A gift from Henry Ho, University of California, Davis, Davis, CA	ATCC Cat# CRL-3216, RRID: CVCL_0063	
Cell line	HeLa cells	A gift from Susan Wente, Vanderbilt University, Nashville, TN	ATCC Cat# CCL-2, RRID: CVCL_0030	
Cell line	hTERT RPE-1 cells	A gift from Irina Kaverina, Vanderbilt University, Nashville, TN	ATCC Cat# CRL-4000, RRID: CVCL_4388	
Software	Fiji (ImageJ)	Image Processing and Analysis in Java	ImageJ, RRID: SCR_002285	
Software	Fusion	Andor Technology, Belfast, UK	Andor Technology	

Software	Imaris	Bitplane, Belfast, UK	Imaris, RRID: SCR_007370	
Software	Jalview	The Barton Group, University of Dundee, Scotland, UK	Jalview, RRID: SCR_006459	
Software	Microsoft Excel	Microsoft, Redmond, WA	Microsoft Excel, RRID: SCR_016137	
Software	Prism 8	Graphpad, San Diego, CA	Graphpad Prism, RRID: SCR_002798	
Software	R	R Project for Statistical Computing	R, RRID: SCR_001905	

Constructs

To generate constructs for stable expression of GFP- or mScarlet-i-PCNT segments controlled by a doxycycline-inducible promoter, each PCNT segment was first amplified by PCR from the pCMV-3xFLAG-EGFP-PCNT-Myc plasmid (a kind gift from Kunsoo Rhee, Seoul National University, Seoul, South Korea) (Lee & Rhee, 2011) and assembled into a vector with sfGFP or mScarlet-i by Gibson assembly (Gibson et al., 2009). The final constructs with the *piggyBac* transposon elements and doxycycline-inducible promoter were made by subcloning the sfGFP- or mScarlet-i-PCNT fragment into PB-TA-ERN (a gift from Knut Woltjen, Addgene plasmid #80474; http://n2t.net/addgene:80474; RRID: Addgene_80474) (Kim et al., 2016) using the Gateway cloning system (Thermo Fisher Scientific, Waltham, MA). The following *piggyBac* transposon constructs, with amino acid sequences of human PCNT in the parentheses, were used in this study: PB-TA-sfGFP-PCNT (2-891), PB-TA-sfGFP-PCNT (854-1960), PB-TA-sfGFP-PCNT (2-1960), and PB-TA-sfGFP-PCNT (1954-3336), PB-TA-mScarlet-i-PCNT (854-1960).

To make the construct to label microtubule plus ends, the EB3-tdTomato fragment was amplified by PCR from the EB3-tdTomato plasmid (a gift from Erik Dent, Addgene plasmid #50708; http://n2t.net/addgene:50708; RRID: Addgene_50708) (Merriam et al., 2013) and cloned into a lentiviral targeting plasmid pLVX-EF1α-mCherry-N1 without the mCherry portion (a gift from Henry Ho, 631986, Takara Bio, Mountain View, CA) by Gibson assembly. The resulting plasmid, pLVX-EF1α-EB3-tdTomato, was used to make lentiviruses to transduce cultured human cells.

To make the construct to label DNA, mScarlet-i-H2A construct was amplified by PCR from the pmScarlet-i_H2A_C1 plasmid (a gift from Dorus Gadella, Addgene plasmid #85053; http://n2t.net/addgene:85053; RRID: Addgene_85053) (Bindels et al., 2017) and cloned into the same lentiviral targeting construct by Gibson assembly as described above to generate pLVX-EF1α-mScarlet-i-H2A.

To make the construct to label the centrioles with far red fluorescence, the coding sequence of human centrin 2 (CETN2) was first cloned from total RNA of HEK293T cells using the SuperScript® III One-Step RT-PCR System (Invitrogen). The miRFP670 was amplified by PCR from the pmiRFP670-N1 plasmid (a gift from Vladislav Verkhusha, Addgene plasmid #79987; http://n2t.net/addgene:79987; RRID: Addgene_79987) (Shcherbakova et al., 2016). miRFP670 and CETN2 were then assembled into the same lentiviral targeting construct by Gibson assembly as described above to generate pLVX-EF1α-miRFP670-CETN2.

To generate the Cas9 tagged with the nuclear localization signal (NLS) at both the N- and C-termini for expression in mammalian cells, an NLS from SV40 large T-antigen (Kalderon et al., 1984) was synthesized and added to hCas9, a construct encoding a human codon-optimized Cas9 (hCas9) with an NLS at its C-terminus (a gift from George Church, Addgene plasmid #41815; http://n2t.net/addgene:41815; RRID: Addgene_41815) (Mali et al., 2013), by PCR. The final construct, pCMVSP6-NLS-hCas9-NLS-polyA_Tol2pA2, with NLS-hCas9-NLS

under the control of the cytomegalovirus (CMV) immediate-early enhancer and promoter was generated by the Gateway cloning system (Thermo Fisher Scientific) using the components from the Tol2kit (Kwan et al., 2007).

Cell culture

RPE-1 cells (a gift from Irina Kaverina, Vanderbilt University) were maintained in Dulbecco's Modification of Eagles Medium/Ham's F-12 50/50 Mix (DMEM/F-12) (10–092-CV, Corning, Corning, NY). HeLa cells (ATCC CCL-2, a gift from Susan Wente, Vanderbilt University, Nashville, TN) and HEK293T cells (a gift from Henry Ho, University of California, Davis, Davis, CA) were maintained in DMEM (10–017-CV, Corning). All cell lines were supplemented with 10% fetal bovine serum (FBS) (12303C, lot no. 13G114, Sigma-Aldrich, St. Louis, MO), 1x Penicillin Streptomycin (30–002 CI, Corning), and maintained in a humidified incubator with 5% CO_2 at 37°C.

Cell lines used in this study were not further authenticated after obtaining from the sources. All cell lines were tested negative for mycoplasma using a PCR-based testing with the Universal Mycoplasma Detection Kit (30–1012K, ATCC, Manassas, VA). None of the cell lines used in this study was included in the list of commonly misidentified cell lines maintained by International Cell Line Authentication Committee.

Generation of GFP-PCNT knock-in cell line

The CRISPR/Cas9 technology with a double-cut homology directed repair (HDR) donor was used to knock in sfGFP into the *PCNT* locus of RPE-1 cells (S. Lin et al., 2014; Zhang et al., 2017). Because it was unclear if knocking in sfGFP would perturb centrosome integrity that might lead to p53-dependent cell cycle arrest (Mikule et al., 2007), making it unfavorable to

isolate the knock-in clones, we first generated a *TP53* knockout RPE-1 cell line before the knock-in experiment (**Figure 1- figure supplement 3**). Knocking out *TP53* was achieved through the CRISPR-mediated gene editing by co-expression of Cas9 protein with the gRNA targeting *TP53* (5'-GGGCAGCTACGGTTTCCGTC-3') using the method described by the Church group (Mali et al., 2013). The gRNA template was cloned into the gRNA Cloning Vector (Addgene plasmid # 41824; http://n2t.net/addgene:41824; RRID: Addgene_41824) via Gibson assembly. 1 μg Cas9 plasmid (pCMVSP6-NLS-hCas9-NLS-polyA_Tol2pA2) and 1 μg gRNA plasmid were transfected into RPE-1 cells using the Lipofectamine P3000 reagent according to the manufacturer's instruction (Invitrogen, Carlsbad, CA). Cells were expanded, isolated as single colonies, and screened for frameshift mutations in both *TP53* alleles by high-throughput Illumina sequencing. The loss of TP53 expression was further confirmed by Western blot analysis. A *TP53*$^{-/-}$;RPE-1 cell line (RPE-1_1-1) was used in this study (**Figure 1- figure supplement 3**).

To knock in sfGFP into the *PCNT* locus, crRNA/tracrRNA (i.e., the Alt-R system, Integrated DNA Technologies, Coralville, IA) were used to target a sequence near the start codon of *PCNT* (CGCGCGGAGTCTGAGGGAGA). The double-cut HDR donor contains the sfGFP-PCNT cassette with 600-bp homology arms flanked by the same guide RNA target sequence (synthesized and cloned into pUC57-Kan vector, Genewiz, South Plainfield, NJ) (**Figure 1-figure supplement 1**). Annealed crRNA/tracrRNA and Cas9 protein (a kind gift from Fuguo Jiang and Jennifer Doudna, Jiang et al., 2016; Jiang et al., 2015) were incubated in 30 mM HEPES, pH 7.5, 1 mM $MgCl_2$, 200 mM KCl, and 1 mM TCEP at 37°C for 10 min to form the Cas9 ribonucleoprotein (RNP) complexes. Before electroporation, the HDR donor plasmid was mixed with 2 x 10^5 of the *TP53*$^{-/-}$;RPE-1 cells synchronized to early M phase using RO-3306 as done before (Sepulveda et al., 2018). The Cas9 RNP complexes were then mixed with the cell/donor vector mix, followed by electroporation using the Neon electroporation system with a

10-μl tip according to the manufacturer's instruction (Pulse voltage: 1200 V, pulse width: 25, pulse number: 4, Invitrogen). The final concentrations of the annealed crRNA/tracrRNA, Cas9 protein, and HDR donor plasmid are 3 μM, 2 μM, and 120 nM, respectively, in a total volume of 10 μl. After electroporation, the cells were grown for 10-14 days in dilute density. Individual clones were isolated and screened for the presence of GFP-positive centrosomes. The GFP-positive clones were further confirmed by anti-PCNT immunostaining and sequencing the junctions of the sfGFP integration site (primer sequences are in **Supplementary file 1**).

Generation of doxycycline-inducible cell lines with GFP- or mScarlet-i-PCNT segments

We used a previously described *piggyBac* transposon system (Kim et al., 2016) to generate stable cell lines that express different GFP- or mScarlet-i-PCNT fusions in a doxycycline-inducible manner. In brief, the PB-TA-sfGFP-PCNT or PB-TA-mScarlet-i-PCNT *piggyBac* transposon construct and a *piggyBac* transposase plasmid (PB210PA-1, System Biosciences, Palo Alto, CA) were electroporated into *TP53*$^{-/-}$;RPE-1 cells using the Neon electroporation system according to the manufacturer's instruction (Invitrogen). After 8-10 day of 200 mg/ml G418 treatment, sfGFP-PCNT integrated cells were obtained. Sometimes fluorescence activated cell sorting (FACS) was further performed to obtain cells with desired, more uniform expression levels of fusion proteins.

Generation of stable cell lines by lentiviral transduction

To generate recombinant lentiviruses expressing EB3-tdTomato, pLVX-EF1α-EB3-tdTomato plasmid was first co-transfected with the following third-generation packaging plasmids (gifts from Didier Trono): pMD2.G (Addgene plasmid #12259; http://n2t.net/addgene:12259; RRID: Addgene_12259), pRSV-rev (Addgene plasmid #12253; http://n2t.net/addgene:12253; RRID:

513 Addgene_12253), and pMDLg/pRRE (Addgene plasmid #12251; http://n2t.net/addgene:12251;
514 RRID: Addgene_12251) (Dull et al., 1998) into HEK293T cells. Viral supernatants were
515 collected from media 24-48 h post transfection, filtered by a 0.22-μm filter, and were used to
516 infect the inducible GFP-PCNT (854-1960) *TP53*$^{-/-}$;RPE-1 cells with 8 μg/ml polybrene. 18-24 h
517 post infection, the viruses were removed and the cells were expanded. To minimize the impact
518 on microtubule dynamics, the cells expressing low levels of EB3-tdTomato (gated and collected
519 by FACS) were used for experiments.

520 To generate lentiviruses expressing mScarlet-i-H2A and miRFP670-CETN2, the same
521 procedure was performed as above except for using the targeting vectors pLVX-EF1α-mScarlet-
522 i-H2A and pLVX-EF1α-miRFP670-CETN2, respectively. The resulting viral supernatants were
523 used to infect the GFP-PCNT knock-in cells as described above.

524

525 **Measurement of protein enrichment in PCNT and HOTag condensates**

526 To test whether the PCNT condensates recruit PCM but exclude non-PCM components,
527 about 5 x 10^4 GFP-PCNT (854-1960) cells were seeded onto each 12-mm circular coverslip in a
528 24-well plate, treated with 1 μg/ml doxycycline treatment for 24 h, followed by immunostaining.
529 To compare the recruitment of PCM component between the PCNT and non-PCNT
530 condensates, the HOTag3/6 condensates (Zhang et al., 2018) were formed by transfecting
531 pcDNA3-FKBP-EGFP-HOTag3 and pcDNA3-Frb-EGFP-HOTag6 plasmids (gifts from Xiaokun
532 Shu; Addgene plasmid #106924 and #106919, respectively) into *TP53*$^{-/-}$;RPE-1 cells using the
533 Lipofectamine P3000 reagent according to the manufacturer's instruction (Invitrogen). In
534 parallel, the doxycycline-inducible GFP-PCNT (854-1960) cells were treated with 1 μg/ml
535 doxycycline for 6 h to induce the formation of PCNT condensates. Cells with either HOTag or

PCNT condensates were then treated with 100 nM rapamycin for 1 h (to induce the formation of HOTag condensates) prior to immunostaining.

Microtubule renucleation assay

Microtubule renucleation assay was adapted from previous studies (Jao et al., 2017; Sanders et al., 2017). In brief, cells were treated with 8.3 μM nocodazole for 2 h to depolymerize microtubules. The plate containing the treated cells was then placed on ice, while washing the cells with ice-cold media for 8 times to remove nocodazole. To allow microtubules to renucleate, the plate was then placed in a 37°C water bath while the cells were incubated with pre-warmed media for 65-110 s (the optimal regrowth period varied between experiments), followed by a 10-s incubation with pre-warmed Extraction Buffer (60 mM PIPES, pH 6.9, 25 mM HEPES, 10 mM EGTA, 2 mM $MgCl_2$, 0.1% Saponin, 0.25 nM nocodazole, 0.25 nM taxol). Immediately after the regrowth, the cells were fixed with 4% paraformaldehyde, 0.025% glutaraldehyde in Cytoskeleton Buffer (10 mM MES, 150 mM NaCl, 5 mM $MgCl_2$, 5 mM EGTA, 5 mM D-glucose) for 10 min at room temperature. The cells were then incubated with 0.2% $NaBH_4$ in 1x PBS for 10 min at room temperature to quench the autofluorescence before immunostaining. For the live MT renucleation assay, the nocodazole-treated EB3-tdTomato-expressing cells with PCNT condensates were mounted on the microscope stage, first imaged in the presence of nocodazole, followed by washes with pre-warmed fresh media 5 times. After washes, the cells were imaged again at 1-min intervals to monitor MT renucleation.

Immunostaining

Immunostaining was performed as previously described (Jiang et al., 2019; Sepulveda et al., 2018). In brief, cells were fixed for 15 min in 4% paraformaldehyde in 1x PBS at room

560 temperature or 5 min in ice-cold 100% methanol at -20°C. Cells were then washed twice with 1x
561 PBS and incubated with Blocking Solution (2% goat serum, 0.1% Triton X-100, and 10 mg/ml
562 bovine serum albumin in 1x PBS) for 1 h at room temperature. Cells were then incubated with
563 Blocking Solution containing diluted primary antibody for 1 h at room temperature, washed three
564 times with 1x PBS, and incubated with Blocking Solution containing diluted secondary antibody
565 for 1 hr at room temperature. Cells were washed three times with 1x PBS, and nuclei were
566 counterstained with 0.05 mg/ml DAPI in 1x PBS for 30 min at room temperature before
567 mounting.
568

569 **Microscopy**

570 Confocal microscopy was performed using a spinning disk confocal microscope system
571 (Dragonfly, Andor Technology, Belfast, UK) housed within a wrap-around incubator (Okolab,
572 Pozzuoli, Italy) with Leica 63x/1.40 or 100x/1.40 HC PL APO objectives, an iXon Ultra 888
573 EMCCD camera, or a Zyla sCMOS camera for immunofluorescence and live cell imaging.
574 Deconvolution was performed using the Fusion software (Andor Technology).
575 For live imaging, cells were seeded in 35-mm glass-bottom dishes 12-18 h prior to imaging
576 and were imaged in a humidified environmental chamber with 5% CO_2 at 37°C.
577 For acute 1,6-hexanediol treatment, 3.5% 1,6-hexanediol in 10% FBS DMEM/F-12 media
578 was added 2 min after the start of time-lapse imaging at 37°C (every 3 min for 5 times; time 0 =
579 the time 1,6-hexanediol was added). Control cells (i.e., no 1,6-hexanediol) were imaged in
580 parallel under the same acquisition condition and intervals.

581 **Fluorescence recovery after photobleaching (FRAP)**

582 A FRAP photoablation module with a computer-controlled fiber optically pumped dye laser
583 was used to bleach a region-of-interest (ROI) on the condensate (~2 μm in diameter) after a few
584 pre-bleach images were acquired. After photobleaching, the same ROI continued to be imaged
585 at 2-s (young condensates) or 5-s (old condensates) intervals for 5 to 12 min. Images were
586 acquired using a Zeiss AxioObserver with a 60x objective coupled with a Yokogawa CSU-10
587 spinning disk confocal system and a Photometrics CoolSNAP HQ2 cooled CCD camera
588 (BioImaging Solutions, San Diego, CA). The microscope system was controlled by Slidebook
589 software (Intelligent Imaging Innovations, Denver, CO) and was enclosed in an environmental
590 chamber with temperature set at 37°C. Images and data were analyzed using ImageJ, Microsoft
591 Excel, and GraphPad Prism 8 (GraphPad, San Diego, CA).
592
593 **Measurement of relative protein concentrations in cells**

594 Doxycycline-inducible cell lines expressing individual GFP-PCNT segments were seeded on
595 glass-bottom 35-mm dishes and live imaging started after addition of 1 μg/ml doxycycline.
596 Imaging of different cell lines was performed with the same acquisition setting and condition (5%
597 CO_2 at 37°C) using a spinning disk confocal microscope system (Dragonfly, Andor Technology).
598 To estimate the relative protein concentrations of GFP-PCNT in cells, the volumes of the
599 condensates and their surrounding cytoplasm were first determined from the confocal voxels.
600 This was done by performing surface rendering of the GFP signals of the condensates (dense
601 phase) and of the whole cytoplasm (light phase) with different thresholds using the Surface
602 reconstruction function of Imaris (Bitplane, Belfast, UK). Depending on the GFP expression level
603 in each cell, threshold values were manually selected for rendering. The volume and intensity
604 sums of each rendered surface were then calculated. The volume and intensity sums in the light

(cytoplasm) phase were calculated by subtracting the values in the dense phase from the total in the cell. Relative protein concentrations were calculated as intensity sum per volume. The critical concentration of phase-separated PCNT segments was determined as the cytoplasmic protein concentration (light phase) of the phase-separated cells since this value stayed relatively constant once the protein phase separated in cells.

Quantification of protein intensity in the condensates

To quantify the fold enrichment of various proteins in the condensates, three randomly chosen fixed areas in the condensates and in the cytoplasm per cell (2.25 μm^2 for data in **Figure 4**, 0.159 μm^2 for data in **Figure 4- figure supplement 1**) were selected for quantification using Fiji. The mean protein intensity value in each selected area was exported into an Excel sheet. The averaged mean intensity values in the cytoplasm and in the condensates per cell were calculated. The fold enrichment in the condensates is calculated as the ratio of protein intensity mean in the condensates per cell to the overall protein intensity mean in the cytoplasm. For cells with centrosomes embedded in the PCNT condensates, PCM protein signals at the centrosomes within the PCNT condensates were excluded from quantification.

Quantification of microtubule density

Each condensate was manually outlined as the first ROI using the freehand selection tool in Fiji. The second ROI was then defined as the cytoplasm space between the outline of the first ROI and the outline 1 μm larger than the first ROI. Values of area and intensity sum of anti-α-tubulin signals in the first (condensate) and second (cytoplasm) ROIs were then calculated in an Excel sheet. One or two condensates was quantified per cell. Microtubule density was calculated as anti-α-tubulin intensity sum per area. Normalized microtubule density was

629 calculated as the ratio of microtubule density in the condensate to the averaged microtubule
630 density in the cytoplasm.
631

632 **Multiple protein sequence alignments**

633 Protein sequences of pericentrin orthologs from a diverse group of vertebrates, as well as
634 two functional homologs of pericentrin from budding yeast (Spc110) and fruit fly (pericentrin-like
635 protein, D-Plp), were retrieved from Ensembl genome database (http://uswest.ensembl.org),
636 resulting in a total of 233 sequences. We further filtered sequences to eliminate those with low-
637 quality sequence reads, incomplete annotations, and those inducing large gaps (e.g., due to the
638 insertions specific to small numbers of species), resulting in a final list of 169 sequences. These
639 169 sequences were then aligned using MUSCLE (Edgar, 2004) and colored with the default
640 Clustal X color scheme in Jalview (**Figure 2- table 1**) (Waterhouse et al., 2009). The
641 conservation of each residue was scored using the AMAS method of multiple sequence
642 alignment analysis in Jalview (Livingstone & Barton, 1993).
643

644 **Statistical analysis**

645 Statistical analysis was performed using the GraphPad Prism 8 (GraphPad). Each sample
646 size (n value) is indicated in the corresponding figure or figure legend. Significance was
647 assessed by performing an unpaired two-sided Student's t-test, as indicated in individual
648 figures. The experiments were not randomized. The investigators were not blinded to allocation
649 during experiments and outcome assessment.

Acknowledgement

We thank Dr. Bo Huang for discussion with the CRISPR knock-in strategy; Dr. Kunsoo Rhee for human PCNT cDNA; Dr. Rick McKenney for the sfGFP construct; Dr. Henry Ho for HEK293T cells, pLVX-EF1α-mCherry-N1, lentiviral packaging plasmids, and critical reading of the manuscript; Dr. Susan Wente for HeLa cells; Dr. Irina Kaverina for RPE-1 cells; Drs. Fuguo Jiang and Jennifer Doudna for Cas9 protein; Dr. Megan Dennis for analyzing Illumina sequencing results; Linhao Jiang for data processing, programming, and analysis of multiple alignment data; Stephen (Evan) Brahms, Marvin Orellana, Hashim Shaikh, Janice Tam, and Alan Zhong for technical help with cell culture work; all members of the Jao and Ho labs for discussion; Emily Jao for help with illustration of the model figure. Experiments were performed in part through the use of Davis Campus Shared Flow Cytometry Resource. The article is dedicated to the memory of Dr. Fuguo Jiang, who recently passed away. Fuguo purified the Cas9 protein and kindly shared it with us for this study.

663 **Legends for movie supplements**

664 **Figure 1- movie supplement 1. A time-lapse movie of a GFP-PCNT knock-in cell.** Part of
665 the time-lapse micrographs (inset #1) are shown in Example 1 of Figure 1. Arrowheads denote
666 the fusing and splitting events of the GFP-PCNT granules. Asterisks denote the centrosomes.
667
668 **Figure 1- movie supplement 2. A time-lapse movie of a GFP-PCNT knock-in cell.** Part of
669 the time-lapse micrographs (inset #1) are shown in Example 2 of Figure 1. Arrowheads denote
670 the fusing and splitting events of the GFP-PCNT granules. Asterisks denote the centrosomes.
671
672 **Figure 1- movie supplement 3. A time-lapse movie of a GFP-PCNT knock-in cell from**
673 **another independent knock-in clone.** Asterisks denote the centrosomes. Note the fusing and
674 splitting events of the GFP-PCNT granules near centrosomes.
675
676 **Figure 2- movie supplement 1. Time-lapse movie of GFP-PCNT (2-1960) condensates in**
677 **RPE-1 cells 24 h post Dox induction.** Part of the time-lapse micrographs (inset #1) are shown
678 in Figure 2C.
679
680 **Figure 2- movie supplement 2. Time-lapse movie of GFP-PCNT (1954-3336) solid-like**
681 **scaffolds in RPE-1 cells 24 h post Dox induction.** Part of the time-lapse micrographs (inset
682 #1) are shown in Figure 2C.
683
684 **Figure 3- movie supplement 1. Time-lapse movie of GFP-PCNT (854-1960) in RPE-1 cells.**
685 Time-lapse imaging started 3.5 h post Dox induction. The centrosomes are labeled by

686 miRFP670-CETN2 fusion protein. Part of the time-lapse micrographs are shown in Figure 3B.

687 GFP-PCNT (854-1960) in yellow, miRFP670-CETN2 in magenta.

688

689 **Figure 3- movie supplement 2. Time-lapse movie of mScarlet-i-PCNT (854-1960) in RPE-1**

690 **cells.** In some cells, the centrosomes are labeled by miRFP670-CETN2 fusion protein.

691 mScarlet-i-PCNT (854-1960) in cyan, miRFP670-CETN2 in magenta.

692 **References**

693

694 Alvarez-Rodrigo, I., Steinacker, T. L., Saurya, S., Conduit, P. T., Baumbach, J., Novak, Z. A.,
695 Aydogan, M. G., Wainman, A., & Raff, J. W. (2019, Sep 9). Evidence that a positive
696 feedback loop drives centrosome maturation in fly embryos. *Elife, 8*, DOI:
697 10.7554/eLife.50130. https://doi.org/10.7554/eLife.50130
698
699 Andersen, J. S., Wilkinson, C. J., Mayor, T., Mortensen, P., Nigg, E. A., & Mann, M. (2003, Dec
700 4). Proteomic characterization of the human centrosome by protein correlation profiling.
701 *Nature, 426*(6966), 570-574. https://doi.org/10.1038/nature02166
702
703 Anitha, A., Nakamura, K., Yamada, K., Iwayama, Y., Toyota, T., Takei, N., Iwata, Y., Suzuki, K.,
704 Sekine, Y., Matsuzaki, H., Kawai, M., Thanseem, I., Miyoshi, K., Katayama, T., Matsuzaki,
705 S., Baba, K., Honda, A., Hattori, T., Shimizu, S., Kumamoto, N., Kikuchi, M., Tohyama, M.,
706 Yoshikawa, T., & Mori, N. (2009, Oct 05). Association studies and gene expression analyses
707 of the DISC1-interacting molecules, pericentrin 2 (PCNT2) and DISC1-binding zinc finger
708 protein (DBZ), with schizophrenia and with bipolar disorder. *Am J Med Genet B*
709 *Neuropsychiatr Genet, 150B*(7), 967-976. https://doi.org/10.1002/ajmg.b.30926
710
711 Anurag, M., Singh, G. P., & Dash, D. (2012, Jan). Location of disorder in coiled coil proteins is
712 influenced by its biological role and subcellular localization: a GO-based study on human
713 proteome. *Mol Biosyst, 8*(1), 346-352. https://doi.org/10.1039/c1mb05210a
714
715 Asherie, N. (2004, Nov). Protein crystallization and phase diagrams. *Methods, 34*(3), 266-272.
716 https://doi.org/10.1016/j.ymeth.2004.03.028
717
718 Atkins, J. D., Boateng, S. Y., Sorensen, T., & McGuffin, L. J. (2015, Aug 13). Disorder Prediction
719 Methods, Their Applicability to Different Protein Targets and Their Usefulness for Guiding
720 Experimental Studies. *Int J Mol Sci, 16*(8), 19040-19054.
721 https://doi.org/10.3390/ijms160819040
722
723 Banani, S. F., Lee, H. O., Hyman, A. A., & Rosen, M. K. (2017, May). Biomolecular
724 condensates: organizers of cellular biochemistry. *Nat Rev Mol Cell Biol, 18*(5), 285-298.
725 https://doi.org/10.1038/nrm.2017.7
726
727 Barr, A. R., & Gergely, F. (2007, Sep 1). Aurora-A: the maker and breaker of spindle poles. *J*
728 *Cell Sci, 120*(Pt 17), 2987-2996. https://doi.org/10.1242/jcs.013136
729
730 Berdnik, D., & Knoblich, J. A. (2002, Apr 16). Drosophila Aurora-A is required for centrosome
731 maturation and actin-dependent asymmetric protein localization during mitosis. *Curr Biol,*
732 *12*(8), 640-647. https://doi.org/10.1016/s0960-9822(02)00766-2
733
734 Berry, J., Weber, S. C., Vaidya, N., Haataja, M., & Brangwynne, C. P. (2015, Sep 22). RNA
735 transcription modulates phase transition-driven nuclear body assembly. *Proc Natl Acad Sci*
736 *U S A, 112*(38), E5237-5245. https://doi.org/10.1073/pnas.1509317112
737
738 Bindels, D. S., Haarbosch, L., van Weeren, L., Postma, M., Wiese, K. E., Mastop, M., Aumonier,
739 S., Gotthard, G., Royant, A., Hink, M. A., & Gadella, T. W., Jr. (2017, Jan). mScarlet: a

bright monomeric red fluorescent protein for cellular imaging. *Nat Methods, 14*(1), 53-56. https://doi.org/10.1038/nmeth.4074

Boeynaems, S., Alberti, S., Fawzi, N. L., Mittag, T., Polymenidou, M., Rousseau, F., Schymkowitz, J., Shorter, J., Wolozin, B., Van Den Bosch, L., Tompa, P., & Fuxreiter, M. (2018, Jun). Protein Phase Separation: A New Phase in Cell Biology. *Trends Cell Biol, 28*(6), 420-435. https://doi.org/10.1016/j.tcb.2018.02.004

Boke, E., Ruer, M., Wuhr, M., Coughlin, M., Lemaitre, R., Gygi, S. P., Alberti, S., Drechsel, D., Hyman, A. A., & Mitchison, T. J. (2016, Jul 28). Amyloid-like Self-Assembly of a Cellular Compartment. *Cell, 166*(3), 637-650. https://doi.org/10.1016/j.cell.2016.06.051

Conduit, P. T., Brunk, K., Dobbelaere, J., Dix, C. I., Lucas, E. P., & Raff, J. W. (2010, Dec 21). Centrioles regulate centrosome size by controlling the rate of Cnn incorporation into the PCM. *Curr Biol, 20*(24), 2178-2186. https://doi.org/10.1016/j.cub.2010.11.011

Conduit, P. T., Feng, Z., Richens, J. H., Baumbach, J., Wainman, A., Bakshi, S. D., Dobbelaere, J., Johnson, S., Lea, S. M., & Raff, J. W. (2014, Mar 31). The centrosome-specific phosphorylation of Cnn by Polo/Plk1 drives Cnn scaffold assembly and centrosome maturation. *Dev Cell, 28*(6), 659-669. https://doi.org/10.1016/j.devcel.2014.02.013

Conduit, P. T., Richens, J. H., Wainman, A., Holder, J., Vicente, C. C., Pratt, M. B., Dix, C. I., Novak, Z. A., Dobbie, I. M., Schermelleh, L., & Raff, J. W. (2014, Aug 22). A molecular mechanism of mitotic centrosome assembly in Drosophila. *Elife, 3*, e03399. https://doi.org/10.7554/eLife.03399

Conduit, P. T., Wainman, A., & Raff, J. W. (2015, Oct). Centrosome function and assembly in animal cells. *Nat Rev Mol Cell Biol, 16*(10), 611-624. https://doi.org/10.1038/nrm4062

Delaval, B., & Doxsey, S. J. (2010, Jan 25). Pericentrin in cellular function and disease. *J Cell Biol, 188*(2), 181-190. https://doi.org/10.1083/jcb.200908114

Dobbelaere, J., Josue, F., Suijkerbuijk, S., Baum, B., Tapon, N., & Raff, J. (2008, Sep 16). A genome-wide RNAi screen to dissect centriole duplication and centrosome maturation in Drosophila. *PLoS Biol, 6*(9), e224. https://doi.org/10.1371/journal.pbio.0060224

Dosztanyi, Z., Csizmok, V., Tompa, P., & Simon, I. (2005, Apr 8). The pairwise energy content estimated from amino acid composition discriminates between folded and intrinsically unstructured proteins. *J Mol Biol, 347*(4), 827-839. https://doi.org/10.1016/j.jmb.2005.01.071

Doxsey, S. (2001, Sep). Re-evaluating centrosome function. *Nat Rev Mol Cell Biol, 2*(9), 688-698. https://doi.org/10.1038/35089575

Dull, T., Zufferey, R., Kelly, M., Mandel, R. J., Nguyen, M., Trono, D., & Naldini, L. (1998, Nov). A third-generation lentivirus vector with a conditional packaging system. *J Virol, 72*(11), 8463-8471. https://www.ncbi.nlm.nih.gov/pubmed/9765382

Edgar, R. C. (2004). MUSCLE: multiple sequence alignment with high accuracy and high throughput. *Nucleic Acids Res, 32*(5), 1792-1797. https://doi.org/10.1093/nar/gkh340

Elbaum-Garfinkle, S., Kim, Y., Szczepaniak, K., Chen, C. C., Eckmann, C. R., Myong, S., & Brangwynne, C. P. (2015, Jun 9). The disordered P granule protein LAF-1 drives phase separation into droplets with tunable viscosity and dynamics. *Proc Natl Acad Sci U S A, 112*(23), 7189-7194. https://doi.org/10.1073/pnas.1504822112

Fang, X., Wang, L., Ishikawa, R., Li, Y., Fiedler, M., Liu, F., Calder, G., Rowan, B., Weigel, D., Li, P., & Dean, C. (2019, May). Arabidopsis FLL2 promotes liquid-liquid phase separation of polyadenylation complexes. *Nature, 569*(7755), 265-269. https://doi.org/10.1038/s41586-019-1165-8

Felix, M. A., Antony, C., Wright, M., & Maro, B. (1994, Jan). Centrosome assembly in vitro: role of gamma-tubulin recruitment in Xenopus sperm aster formation. *J Cell Biol, 124*(1-2), 19-31. https://doi.org/10.1083/jcb.124.1.19

Feng, Z., Caballe, A., Wainman, A., Johnson, S., Haensele, A. F. M., Cottee, M. A., Conduit, P. T., Lea, S. M., & Raff, J. W. (2017, Jun 1). Structural Basis for Mitotic Centrosome Assembly in Flies. *Cell, 169*(6), 1078-1089 e1013. https://doi.org/10.1016/j.cell.2017.05.030

Fu, J., & Glover, D. M. (2012, Aug). Structured illumination of the interface between centriole and peri-centriolar material. *Open Biol, 2*(8), 120104. https://doi.org/10.1098/rsob.120104

Galati, D. F., Sullivan, K. D., Pham, A. T., Espinosa, J. M., & Pearson, C. G. (2018, Sep 10). Trisomy 21 Represses Cilia Formation and Function. *Dev Cell, 46*(5), 641-650 e646. https://doi.org/10.1016/j.devcel.2018.07.008

Gibson, D. G., Young, L., Chuang, R. Y., Venter, J. C., Hutchison, C. A., 3rd, & Smith, H. O. (2009, May). Enzymatic assembly of DNA molecules up to several hundred kilobases. *Nat Methods, 6*(5), 343-345. https://doi.org/10.1038/nmeth.1318

Gillingham, A. K., & Munro, S. (2000, Dec). The PACT domain, a conserved centrosomal targeting motif in the coiled-coil proteins AKAP450 and pericentrin. *EMBO Rep, 1*(6), 524-529. https://doi.org/10.1093/embo-reports/kvd105

Goshima, G., Wollman, R., Goodwin, S. S., Zhang, N., Scholey, J. M., Vale, R. D., & Stuurman, N. (2007, Apr 20). Genes required for mitotic spindle assembly in Drosophila S2 cells. *Science, 316*(5823), 417-421. https://doi.org/10.1126/science.1141314

Griffith, E., Walker, S., Martin, C. A., Vagnarelli, P., Stiff, T., Vernay, B., Al Sanna, N., Saggar, A., Hamel, B., Earnshaw, W. C., Jeggo, P. A., Jackson, A. P., & O'Driscoll, M. (2008, Feb). Mutations in pericentrin cause Seckel syndrome with defective ATR-dependent DNA damage signaling. *Nat Genet, 40*(2), 232-236. https://doi.org/10.1038/ng.2007.80

Grigoryan, G., & Keating, A. E. (2008, Aug). Structural specificity in coiled-coil interactions. *Curr Opin Struct Biol, 18*(4), 477-483. https://doi.org/10.1016/j.sbi.2008.04.008

Grigoryan, G., Kim, Y. H., Acharya, R., Axelrod, K., Jain, R. M., Willis, L., Drndic, M., Kikkawa, J. M., & DeGrado, W. F. (2011, May 27). Computational design of virus-like protein

assemblies on carbon nanotube surfaces. *Science, 332*(6033), 1071-1076. https://doi.org/10.1126/science.1198841

Gupta, G. D., & Pelletier, L. (2017, Sep 11). Centrosome Biology: Polymer-Based Centrosome Maturation. *Curr Biol, 27*(17), R836-R839. https://doi.org/10.1016/j.cub.2017.07.036

Hamill, D. R., Severson, A. F., Carter, J. C., & Bowerman, B. (2002, Nov). Centrosome maturation and mitotic spindle assembly in C. elegans require SPD-5, a protein with multiple coiled-coil domains. *Dev Cell, 3*(5), 673-684. https://www.ncbi.nlm.nih.gov/pubmed/12431374

Hannak, E., Kirkham, M., Hyman, A. A., & Oegema, K. (2001, Dec 24). Aurora-A kinase is required for centrosome maturation in Caenorhabditis elegans. *J Cell Biol, 155*(7), 1109-1116. https://doi.org/10.1083/jcb.200108051

Hannak, E., Oegema, K., Kirkham, M., Gonczy, P., Habermann, B., & Hyman, A. A. (2002, May 13). The kinetically dominant assembly pathway for centrosomal asters in Caenorhabditis elegans is gamma-tubulin dependent. *J Cell Biol, 157*(4), 591-602. https://doi.org/10.1083/jcb.200202047

Haren, L., Stearns, T., & Luders, J. (2009, Jun 19). Plk1-dependent recruitment of gamma-tubulin complexes to mitotic centrosomes involves multiple PCM components. *PLoS One, 4*(6), e5976. https://doi.org/10.1371/journal.pone.0005976

Hennig, S., Kong, G., Mannen, T., Sadowska, A., Kobelke, S., Blythe, A., Knott, G. J., Iyer, K. S., Ho, D., Newcombe, E. A., Hosoki, K., Goshima, N., Kawaguchi, T., Hatters, D., Trinkle-Mulcahy, L., Hirose, T., Bond, C. S., & Fox, A. H. (2015, Aug 17). Prion-like domains in RNA binding proteins are essential for building subnuclear paraspeckles. *J Cell Biol, 210*(4), 529-539. https://doi.org/10.1083/jcb.201504117

Holehouse, A. S., & Pappu, R. V. (2018, May 1). Functional Implications of Intracellular Phase Transitions. *Biochemistry, 57*(17), 2415-2423. https://doi.org/10.1021/acs.biochem.7b01136

Huang, P. S., Oberdorfer, G., Xu, C., Pei, X. Y., Nannenga, B. L., Rogers, J. M., DiMaio, F., Gonen, T., Luisi, B., & Baker, D. (2014, Oct 24). High thermodynamic stability of parametrically designed helical bundles. *Science, 346*(6208), 481-485. https://doi.org/10.1126/science.1257481

Hutchins, J. R., Toyoda, Y., Hegemann, B., Poser, I., Heriche, J. K., Sykora, M. M., Augsburg, M., Hudecz, O., Buschhorn, B. A., Bulkescher, J., Conrad, C., Comartin, D., Schleiffer, A., Sarov, M., Pozniakovsky, A., Slabicki, M. M., Schloissnig, S., Steinmacher, I., Leuschner, M., Ssykor, A., Lawo, S., Pelletier, L., Stark, H., Nasmyth, K., Ellenberg, J., Durbin, R., Buchholz, F., Mechtler, K., Hyman, A. A., & Peters, J. M. (2010, Apr 30). Systematic analysis of human protein complexes identifies chromosome segregation proteins. *Science, 328*(5978), 593-599. https://doi.org/10.1126/science.1181348

Hyman, A. A., Weber, C. A., & Julicher, F. (2014). Liquid-liquid phase separation in biology. *Annu Rev Cell Dev Biol, 30*, 39-58. https://doi.org/10.1146/annurev-cellbio-100913-013325

886 Jao, L. E., Akef, A., & Wente, S. R. (2017, Jan 01). A role for Gle1, a regulator of DEAD-box
887 RNA helicases, at centrosomes and basal bodies. *Mol Biol Cell, 28*(1), 120-127.
888 https://doi.org/10.1091/mbc.E16-09-0675
889
890 Jeng, R., & Stearns, T. (1999, Sep). Gamma-tubulin complexes: size does matter. *Trends Cell*
891 *Biol, 9*(9), 339-342. https://www.ncbi.nlm.nih.gov/pubmed/10461186
892
893 Jiang, F., Taylor, D. W., Chen, J. S., Kornfeld, J. E., Zhou, K., Thompson, A. J., Nogales, E., &
894 Doudna, J. A. (2016, Feb 19). Structures of a CRISPR-Cas9 R-loop complex primed for
895 DNA cleavage. *Science, 351*(6275), 867-871. https://doi.org/10.1126/science.aad8282
896
897 Jiang, F., Zhou, K., Ma, L., Gressel, S., & Doudna, J. A. (2015, Jun 26). A Cas9-guide RNA
898 complex preorganized for target DNA recognition. *Science, 348*(6242), 1477-1481.
899 https://doi.org/10.1126/science.aab1452
900
901 Jiang, X., Brust-Mascher, I., & Jao, L. E. (2019, Aug 20). Three-dimensional reconstruction and
902 quantification of proteins and mRNAs at the single-cell level in cultured cells. *Bio-protocol,*
903 *9*(16), e3330. https://doi.org/10.21769/BioProtoc.3330
904
905 Joshi, H. C., Palacios, M. J., McNamara, L., & Cleveland, D. W. (1992, Mar 5). Gamma-tubulin
906 is a centrosomal protein required for cell cycle-dependent microtubule nucleation. *Nature,*
907 *356*(6364), 80-83. https://doi.org/10.1038/356080a0
908
909 Joukov, V., Walter, J. C., & De Nicolo, A. (2014, Aug 21). The Cep192-organized aurora A-Plk1
910 cascade is essential for centrosome cycle and bipolar spindle assembly. *Mol Cell, 55*(4),
911 578-591. https://doi.org/10.1016/j.molcel.2014.06.016
912
913 Kalderon, D., Roberts, B. L., Richardson, W. D., & Smith, A. E. (1984, Dec). A short amino acid
914 sequence able to specify nuclear location. *Cell, 39*(3 Pt 2), 499-509.
915 https://doi.org/10.1016/0092-8674(84)90457-4
916
917 Kato, M., Han, T. W., Xie, S., Shi, K., Du, X., Wu, L. C., Mirzaei, H., Goldsmith, E. J., Longgood,
918 J., Pei, J., Grishin, N. V., Frantz, D. E., Schneider, J. W., Chen, S., Li, L., Sawaya, M. R.,
919 Eisenberg, D., Tycko, R., & McKnight, S. L. (2012, May 11). Cell-free formation of RNA
920 granules: low complexity sequence domains form dynamic fibers within hydrogels. *Cell,*
921 *149*(4), 753-767. https://doi.org/10.1016/j.cell.2012.04.017
922
923 Kemp, C. A., Kopish, K. R., Zipperlen, P., Ahringer, J., & O'Connell, K. F. (2004, Apr).
924 Centrosome maturation and duplication in C. elegans require the coiled-coil protein SPD-2.
925 *Dev Cell, 6*(4), 511-523. https://www.ncbi.nlm.nih.gov/pubmed/15068791
926
927 Khodjakov, A., & Rieder, C. L. (1999, Aug 09). The sudden recruitment of gamma-tubulin to the
928 centrosome at the onset of mitosis and its dynamic exchange throughout the cell cycle, do
929 not require microtubules. *J Cell Biol, 146*(3), 585-596.
930 https://www.ncbi.nlm.nih.gov/pubmed/10444067
931
932 Kim, S., & Rhee, K. (2014). Importance of the CEP215-pericentrin interaction for centrosome
933 maturation during mitosis. *PLoS One, 9*(1), e87016.
934 https://doi.org/10.1371/journal.pone.0087016

Kim, S. I., Oceguera-Yanez, F., Sakurai, C., Nakagawa, M., Yamanaka, S., & Woltjen, K. (2016). Inducible Transgene Expression in Human iPS Cells Using Versatile All-in-One piggyBac Transposons. *Methods Mol Biol, 1357*, 111-131. https://doi.org/10.1007/7651_2015_251

Kinoshita, K., Noetzel, T. L., Pelletier, L., Mechtler, K., Drechsel, D. N., Schwager, A., Lee, M., Raff, J. W., & Hyman, A. A. (2005, Sep 26). Aurora A phosphorylation of TACC3/maskin is required for centrosome-dependent microtubule assembly in mitosis. *J Cell Biol, 170*(7), 1047-1055. https://doi.org/10.1083/jcb.200503023

Knop, M., & Schiebel, E. (1997, Dec 1). Spc98p and Spc97p of the yeast gamma-tubulin complex mediate binding to the spindle pole body via their interaction with Spc110p. *EMBO J, 16*(23), 6985-6995. https://doi.org/10.1093/emboj/16.23.6985

Kroschwald, S., Maharana, S., & Simon, A. (2017). Hexanediol: a chemical probe to investigate the material properties of membrane-less compartments. *Matters*. https://doi.org/10.19185/matters.201702000010

Kwan, K. M., Fujimoto, E., Grabher, C., Mangum, B. D., Hardy, M. E., Campbell, D. S., Parant, J. M., Yost, H. J., Kanki, J. P., & Chien, C. B. (2007, Nov). The Tol2kit: a multisite gateway-based construction kit for Tol2 transposon transgenesis constructs. *Dev Dyn, 236*(11), 3088-3099. https://doi.org/10.1002/dvdy.21343

Larson, A. G., Elnatan, D., Keenen, M. M., Trnka, M. J., Johnston, J. B., Burlingame, A. L., Agard, D. A., Redding, S., & Narlikar, G. J. (2017, Jul 13). Liquid droplet formation by HP1alpha suggests a role for phase separation in heterochromatin. *Nature, 547*(7662), 236-240. https://doi.org/10.1038/nature22822

Lawo, S., Hasegan, M., Gupta, G. D., & Pelletier, L. (2012, Nov). Subdiffraction imaging of centrosomes reveals higher-order organizational features of pericentriolar material. *Nat Cell Biol, 14*(11), 1148-1158. https://doi.org/10.1038/ncb2591

Lee, K., & Rhee, K. (2011, Dec 26). PLK1 phosphorylation of pericentrin initiates centrosome maturation at the onset of mitosis. *J Cell Biol, 195*(7), 1093-1101. https://doi.org/10.1083/jcb.201106093

Li, Y., Brown, J. H., Reshetnikova, L., Blazsek, A., Farkas, L., Nyitray, L., & Cohen, C. (2003, Jul 17). Visualization of an unstable coiled coil from the scallop myosin rod. *Nature, 424*(6946), 341-345. https://doi.org/10.1038/nature01801

Lin, S., Staahl, B. T., Alla, R. K., & Doudna, J. A. (2014, Dec 15). Enhanced homology-directed human genome engineering by controlled timing of CRISPR/Cas9 delivery. *Elife, 3*, e04766. https://doi.org/10.7554/eLife.04766

Lin, T. C., Neuner, A., Schlosser, Y. T., Scharf, A. N., Weber, L., & Schiebel, E. (2014, Apr 30). Cell-cycle dependent phosphorylation of yeast pericentrin regulates gamma-TuSC-mediated microtubule nucleation. *Elife, 3*, e02208. https://doi.org/10.7554/eLife.02208

Lin, Y., Protter, D. S., Rosen, M. K., & Parker, R. (2015, Oct 15). Formation and Maturation of Phase-Separated Liquid Droplets by RNA-Binding Proteins. *Mol Cell, 60*(2), 208-219. https://doi.org/10.1016/j.molcel.2015.08.018

Lindsay, H., Burger, A., Biyong, B., Felker, A., Hess, C., Zaugg, J., Chiavacci, E., Anders, C., Jinek, M., Mosimann, C., & Robinson, M. D. (2016, Jul 12). CrispRVariants charts the mutation spectrum of genome engineering experiments. *Nat Biotechnol, 34*(7), 701-702. https://doi.org/10.1038/nbt.3628

Livingstone, C. D., & Barton, G. J. (1993, Dec). Protein sequence alignments: a strategy for the hierarchical analysis of residue conservation. *Comput Appl Biosci, 9*(6), 745-756. https://doi.org/10.1093/bioinformatics/9.6.745

Lu, Y., Wu, T., Gutman, O., Lu, H., Zhou, Q., Henis, Y. I., & Luo, K. (2020, Mar 23). Phase separation of TAZ compartmentalizes the transcription machinery to promote gene expression. *Nat Cell Biol*. https://doi.org/10.1038/s41556-020-0485-0

Lupas, A., Van Dyke, M., & Stock, J. (1991, May 24). Predicting coiled coils from protein sequences. *Science, 252*(5009), 1162-1164. https://doi.org/10.1126/science.252.5009.1162

Mahen, R., & Venkitaraman, A. R. (2012, Feb). Pattern formation in centrosome assembly. *Curr Opin Cell Biol, 24*(1), 14-23. https://doi.org/10.1016/j.ceb.2011.12.012

Mali, P., Yang, L., Esvelt, K. M., Aach, J., Guell, M., DiCarlo, J. E., Norville, J. E., & Church, G. M. (2013, Feb 15). RNA-guided human genome engineering via Cas9. *Science, 339*(6121), 823-826. https://doi.org/10.1126/science.1232033

Martinez-Campos, M., Basto, R., Baker, J., Kernan, M., & Raff, J. W. (2004, Jun 7). The Drosophila pericentrin-like protein is essential for cilia/flagella function, but appears to be dispensable for mitosis. *J Cell Biol, 165*(5), 673-683. https://doi.org/10.1083/jcb.200402130

Meng, L., Park, J. E., Kim, T. S., Lee, E. H., Park, S. Y., Zhou, M., Bang, J. K., & Lee, K. S. (2015, Aug). Bimodal Interaction of Mammalian Polo-Like Kinase 1 and a Centrosomal Scaffold, Cep192, in the Regulation of Bipolar Spindle Formation. *Mol Cell Biol, 35*(15), 2626-2640. https://doi.org/10.1128/MCB.00068-15

Mennella, V., Agard, D. A., Huang, B., & Pelletier, L. (2014, Mar). Amorphous no more: subdiffraction view of the pericentriolar material architecture. *Trends Cell Biol, 24*(3), 188-197. https://doi.org/10.1016/j.tcb.2013.10.001

Mennella, V., Keszthelyi, B., McDonald, K. L., Chhun, B., Kan, F., Rogers, G. C., Huang, B., & Agard, D. A. (2012, Nov). Subdiffraction-resolution fluorescence microscopy reveals a domain of the centrosome critical for pericentriolar material organization. *Nat Cell Biol, 14*(11), 1159-1168. https://doi.org/10.1038/ncb2597

Merriam, E. B., Millette, M., Lumbard, D. C., Saengsawang, W., Fothergill, T., Hu, X., Ferhat, L., & Dent, E. W. (2013, Oct 16). Synaptic regulation of microtubule dynamics in dendritic spines by calcium, F-actin, and drebrin. *J Neurosci, 33*(42), 16471-16482. https://doi.org/10.1523/JNEUROSCI.0661-13.2013

Mikule, K., Delaval, B., Kaldis, P., Jurcyzk, A., Hergert, P., & Doxsey, S. (2007, Feb). Loss of centrosome integrity induces p38-p53-p21-dependent G1-S arrest. *Nat Cell Biol, 9*(2), 160-170. https://doi.org/10.1038/ncb1529

Molliex, A., Temirov, J., Lee, J., Coughlin, M., Kanagaraj, A. P., Kim, H. J., Mittag, T., & Taylor, J. P. (2015, Sep 24). Phase separation by low complexity domains promotes stress granule assembly and drives pathological fibrillization. *Cell, 163*(1), 123-133. https://doi.org/10.1016/j.cell.2015.09.015

Moritz, M., Braunfeld, M. B., Fung, J. C., Sedat, J. W., Alberts, B. M., & Agard, D. A. (1995, Sep). Three-dimensional structural characterization of centrosomes from early Drosophila embryos. *J Cell Biol, 130*(5), 1149-1159. https://doi.org/10.1083/jcb.130.5.1149

Moritz, M., Braunfeld, M. B., Sedat, J. W., Alberts, B., & Agard, D. A. (1995, Dec 07). Microtubule nucleation by gamma-tubulin-containing rings in the centrosome. *Nature, 378*(6557), 638-640. https://doi.org/10.1038/378638a0

Moritz, M., Zheng, Y., Alberts, B. M., & Oegema, K. (1998, Aug 10). Recruitment of the gamma-tubulin ring complex to Drosophila salt-stripped centrosome scaffolds. *J Cell Biol, 142*(3), 775-786. https://doi.org/10.1083/jcb.142.3.775

Neumann, B., Walter, T., Heriche, J. K., Bulkescher, J., Erfle, H., Conrad, C., Rogers, P., Poser, I., Held, M., Liebel, U., Cetin, C., Sieckmann, F., Pau, G., Kabbe, R., Wunsche, A., Satagopam, V., Schmitz, M. H., Chapuis, C., Gerlich, D. W., Schneider, R., Eils, R., Huber, W., Peters, J. M., Hyman, A. A., Durbin, R., Pepperkok, R., & Ellenberg, J. (2010, Apr 01). Phenotypic profiling of the human genome by time-lapse microscopy reveals cell division genes. *Nature, 464*(7289), 721-727. https://doi.org/10.1038/nature08869

Nott, T. J., Petsalaki, E., Farber, P., Jervis, D., Fussner, E., Plochowietz, A., Craggs, T. D., Bazett-Jones, D. P., Pawson, T., Forman-Kay, J. D., & Baldwin, A. J. (2015, Mar 5). Phase transition of a disordered nuage protein generates environmentally responsive membraneless organelles. *Mol Cell, 57*(5), 936-947. https://doi.org/10.1016/j.molcel.2015.01.013

Numata, S., Iga, J., Nakataki, M., Tayoshi, S., Tanahashi, T., Itakura, M., Ueno, S., & Ohmori, T. (2009, May). Positive association of the pericentrin (PCNT) gene with major depressive disorder in the Japanese population. *J Psychiatry Neurosci, 34*(3), 195-198. https://www.ncbi.nlm.nih.gov/pubmed/19448849

Oakley, B. R., Oakley, C. E., Yoon, Y., & Jung, M. K. (1990, Jun 29). Gamma-tubulin is a component of the spindle pole body that is essential for microtubule function in Aspergillus nidulans. *Cell, 61*(7), 1289-1301. https://doi.org/10.1016/0092-8674(90)90693-9

Oegema, K., Wiese, C., Martin, O. C., Milligan, R. A., Iwamatsu, A., Mitchison, T. J., & Zheng, Y. (1999, Feb 22). Characterization of two related Drosophila gamma-tubulin complexes that differ in their ability to nucleate microtubules. *J Cell Biol, 144*(4), 721-733. https://doi.org/10.1083/jcb.144.4.721

Palazzo, R. E., Vogel, J. M., Schnackenberg, B. J., Hull, D. R., & Wu, X. (2000). Centrosome maturation. *Curr Top Dev Biol, 49*, 449-470. https://www.ncbi.nlm.nih.gov/pubmed/11005031

Patel, A., Lee, H. O., Jawerth, L., Maharana, S., Jahnel, M., Hein, M. Y., Stoynov, S., Mahamid, J., Saha, S., Franzmann, T. M., Pozniakovski, A., Poser, I., Maghelli, N., Royer, L. A., Weigert, M., Myers, E. W., Grill, S., Drechsel, D., Hyman, A. A., & Alberti, S. (2015, Aug 27). A Liquid-to-Solid Phase Transition of the ALS Protein FUS Accelerated by Disease Mutation. *Cell, 162*(5), 1066-1077. https://doi.org/10.1016/j.cell.2015.07.047

Peng, K., Radivojac, P., Vucetic, S., Dunker, A. K., & Obradovic, Z. (2006, Apr 17). Length-dependent prediction of protein intrinsic disorder. *BMC Bioinformatics, 7*, 208. https://doi.org/10.1186/1471-2105-7-208

Peng, K., Vucetic, S., Radivojac, P., Brown, C. J., Dunker, A. K., & Obradovic, Z. (2005, Feb). Optimizing long intrinsic disorder predictors with protein evolutionary information. *J Bioinform Comput Biol, 3*(1), 35-60. https://doi.org/10.1142/s0219720005000886

Piehl, M., Tulu, U. S., Wadsworth, P., & Cassimeris, L. (2004, Feb 10). Centrosome maturation: measurement of microtubule nucleation throughout the cell cycle by using GFP-tagged EB1. *Proc Natl Acad Sci U S A, 101*(6), 1584-1588. https://doi.org/10.1073/pnas.0308205100

Raff, J. W. (2019, May 7). Phase Separation and the Centrosome: A Fait Accompli? *Trends Cell Biol*. https://doi.org/10.1016/j.tcb.2019.04.001

Rauch, A., Thiel, C. T., Schindler, D., Wick, U., Crow, Y. J., Ekici, A. B., van Essen, A. J., Goecke, T. O., Al-Gazali, L., Chrzanowska, K. H., Zweier, C., Brunner, H. G., Becker, K., Curry, C. J., Dallapiccola, B., Devriendt, K., Dorfler, A., Kinning, E., Megarbane, A., Meinecke, P., Semple, R. K., Spranger, S., Toutain, A., Trembath, R. C., Voss, E., Wilson, L., Hennekam, R., de Zegher, F., Dorr, H. G., & Reis, A. (2008, Feb 8). Mutations in the pericentrin (PCNT) gene cause primordial dwarfism. *Science, 319*(5864), 816-819. https://doi.org/10.1126/science.1151174

Riback, J. A., Katanski, C. D., Kear-Scott, J. L., Pilipenko, E. V., Rojek, A. E., Sosnick, T. R., & Drummond, D. A. (2017, Mar 9). Stress-Triggered Phase Separation Is an Adaptive, Evolutionarily Tuned Response. *Cell, 168*(6), 1028-1040 e1019. https://doi.org/10.1016/j.cell.2017.02.027

Ribbeck, K., & Gorlich, D. (2002, Jun 3). The permeability barrier of nuclear pore complexes appears to operate via hydrophobic exclusion. *EMBO J, 21*(11), 2664-2671. https://doi.org/10.1093/emboj/21.11.2664

Rieder, C. L., & Borisy, G. G. (1982). The centrosome cycle in PtK2 cells: Asymmetric distribution and structural changes in the pericentriolar material. *Biology of the Cell, 44*, 117-132.

Romero, P., Obradovic, Z., & Dunker, A. K. (1999, Dec 3). Folding minimal sequences: the lower bound for sequence complexity of globular proteins. *FEBS Lett, 462*(3), 363-367. https://doi.org/10.1016/s0014-5793(99)01557-4

Rose, A., & Meier, I. (2004, Aug). Scaffolds, levers, rods and springs: diverse cellular functions of long coiled-coil proteins. *Cell Mol Life Sci, 61*(16), 1996-2009. https://doi.org/10.1007/s00018-004-4039-6

Salisbury, J. L. (2003, Feb 4). Centrosomes: coiled-coils organize the cell center. *Curr Biol, 13*(3), R88-90. https://doi.org/10.1016/s0960-9822(03)00033-2

Sanders, A., Chang, K., Zhu, X., Thoppil, R. J., Holmes, W. R., & Kaverina, I. (2017, Nov 7). Nonrandom gamma-TuNA-dependent spatial pattern of microtubule nucleation at the Golgi. *Mol Biol Cell, 28*(23), 3181-3192. https://doi.org/10.1091/mbc.E17-06-0425

Schnackenberg, B. J., Khodjakov, A., Rieder, C. L., & Palazzo, R. E. (1998, Aug 4). The disassembly and reassembly of functional centrosomes in vitro. *Proc Natl Acad Sci U S A, 95*(16), 9295-9300. https://doi.org/10.1073/pnas.95.16.9295

Schnackenberg, B. J., & Palazzo, R. E. (1999, Jul). Identification and function of the centrosome centromatrix. *Biol Cell, 91*(6), 429-438. https://www.ncbi.nlm.nih.gov/pubmed/10576861

Sepulveda, G., Antkowiak, M., Brust-Mascher, I., Mahe, K., Ou, T., Castro, N. M., Christensen, L. N., Cheung, L., Jiang, X., Yoon, D., Huang, B., & Jao, L. E. (2018, Apr 30). Co-translational protein targeting facilitates centrosomal recruitment of PCNT during centrosome maturation in vertebrates. *Elife, 7*, pii: e34959. doi: 34910.37554/eLife.34959. https://doi.org/10.7554/eLife.34959

Shcherbakova, D. M., Baloban, M., Emelyanov, A. V., Brenowitz, M., Guo, P., & Verkhusha, V. V. (2016, Aug 19). Bright monomeric near-infrared fluorescent proteins as tags and biosensors for multiscale imaging. *Nat Commun, 7*, 12405. https://doi.org/10.1038/ncomms12405

Shin, Y., & Brangwynne, C. P. (2017, Sep 22). Liquid phase condensation in cell physiology and disease. *Science, 357*(6357). https://doi.org/10.1126/science.aaf4382

Smith, J., Calidas, D., Schmidt, H., Lu, T., Rasoloson, D., & Seydoux, G. (2016, Dec 3). Spatial patterning of P granules by RNA-induced phase separation of the intrinsically-disordered protein MEG-3. *Elife, 5*. https://doi.org/10.7554/eLife.21337

So, C., Seres, K. B., Steyer, A. M., Monnich, E., Clift, D., Pejkovska, A., Mobius, W., & Schuh, M. (2019, Jun 28). A liquid-like spindle domain promotes acentrosomal spindle assembly in mammalian oocytes. *Science, 364*(6447). https://doi.org/10.1126/science.aat9557

Sonnen, K. F., Schermelleh, L., Leonhardt, H., & Nigg, E. A. (2012, Oct 15). 3D-structured illumination microscopy provides novel insight into architecture of human centrosomes. *Biol Open, 1*(10), 965-976. https://doi.org/10.1242/bio.20122337

Sonnichsen, B., Koski, L. B., Walsh, A., Marschall, P., Neumann, B., Brehm, M., Alleaume, A. M., Artelt, J., Bettencourt, P., Cassin, E., Hewitson, M., Holz, C., Khan, M., Lazik, S., Martin, C., Nitzsche, B., Ruer, M., Stamford, J., Winzi, M., Heinkel, R., Roder, M., Finell, J., Hantsch, H., Jones, S. J., Jones, M., Piano, F., Gunsalus, K. C., Oegema, K., Gonczy, P.,

Coulson, A., Hyman, A. A., & Echeverri, C. J. (2005, Mar 24). Full-genome RNAi profiling of early embryogenesis in Caenorhabditis elegans. *Nature, 434*(7032), 462-469. https://doi.org/10.1038/nature03353

Stearns, T., Evans, L., & Kirschner, M. (1991, May 31). Gamma-tubulin is a highly conserved component of the centrosome. *Cell, 65*(5), 825-836. https://doi.org/10.1016/0092-8674(91)90390-k

Stearns, T., & Kirschner, M. (1994, Feb 25). In vitro reconstitution of centrosome assembly and function: the central role of gamma-tubulin. *Cell, 76*(4), 623-637. https://doi.org/10.1016/0092-8674(94)90503-7

Strom, A. R., Emelyanov, A. V., Mir, M., Fyodorov, D. V., Darzacq, X., & Karpen, G. H. (2017, Jul 13). Phase separation drives heterochromatin domain formation. *Nature, 547*(7662), 241-245. https://doi.org/10.1038/nature22989

Sundberg, H. A., & Davis, T. N. (1997, Dec). A mutational analysis identifies three functional regions of the spindle pole component Spc110p in Saccharomyces cerevisiae. *Mol Biol Cell, 8*(12), 2575-2590. https://doi.org/10.1091/mbc.8.12.2575

Szappanos, B., Suveges, D., Nyitray, L., Perczel, A., & Gaspari, Z. (2010, Apr 16). Folded-unfolded cross-predictions and protein evolution: the case study of coiled-coils. *FEBS Lett, 584*(8), 1623-1627. https://doi.org/10.1016/j.febslet.2010.03.026

Takahashi, M., Yamagiwa, A., Nishimura, T., Mukai, H., & Ono, Y. (2002, Sep). Centrosomal proteins CG-NAP and kendrin provide microtubule nucleation sites by anchoring gamma-tubulin ring complex. *Mol Biol Cell, 13*(9), 3235-3245. https://doi.org/10.1091/mbc.e02-02-0112

Thomson, A. R., Wood, C. W., Burton, A. J., Bartlett, G. J., Sessions, R. B., Brady, R. L., & Woolfson, D. N. (2014, Oct 24). Computational design of water-soluble alpha-helical barrels. *Science, 346*(6208), 485-488. https://doi.org/10.1126/science.1257452

Tynan, S. H., Purohit, A., Doxsey, S. J., & Vallee, R. B. (2000, Oct 20). Light intermediate chain 1 defines a functional subfraction of cytoplasmic dynein which binds to pericentrin. *J Biol Chem, 275*(42), 32763-32768. https://doi.org/10.1074/jbc.M001536200

Uversky, V. N., Gillespie, J. R., & Fink, A. L. (2000, Nov 15). Why are "natively unfolded" proteins unstructured under physiologic conditions? *Proteins, 41*(3), 415-427. https://doi.org/10.1002/1097-0134(20001115)41:3<415::aid-prot130>3.0.co;2-7

Vega, I. E., Umstead, A., & Kanaan, N. M. (2019). EFhd2 Affects Tau Liquid-Liquid Phase Separation. *Front Neurosci, 13*, 845. https://doi.org/10.3389/fnins.2019.00845

Vorobjev, I. A., & Chentsov Yu, S. (1982, Jun). Centrioles in the cell cycle. I. Epithelial cells. *J Cell Biol, 93*(3), 938-949. https://doi.org/10.1083/jcb.93.3.938

Wang, J., Choi, J. M., Holehouse, A. S., Lee, H. O., Zhang, X., Jahnel, M., Maharana, S., Lemaitre, R., Pozniakovsky, A., Drechsel, D., Poser, I., Pappu, R. V., Alberti, S., & Hyman,

A. A. (2018, Jul 26). A Molecular Grammar Governing the Driving Forces for Phase Separation of Prion-like RNA Binding Proteins. *Cell, 174*(3), 688-699 e616. https://doi.org/10.1016/j.cell.2018.06.006

Wang, W. J., Soni, R. K., Uryu, K., & Tsou, M. F. (2011, May 16). The conversion of centrioles to centrosomes: essential coupling of duplication with segregation. *J Cell Biol, 193*(4), 727-739. https://doi.org/10.1083/jcb.201101109

Waterhouse, A. M., Procter, J. B., Martin, D. M., Clamp, M., & Barton, G. J. (2009, May 1). Jalview Version 2--a multiple sequence alignment editor and analysis workbench. *Bioinformatics, 25*(9), 1189-1191. https://doi.org/10.1093/bioinformatics/btp033

Wegmann, S., Eftekharzadeh, B., Tepper, K., Zoltowska, K. M., Bennett, R. E., Dujardin, S., Laskowski, P. R., MacKenzie, D., Kamath, T., Commins, C., Vanderburg, C., Roe, A. D., Fan, Z., Molliex, A. M., Hernandez-Vega, A., Muller, D., Hyman, A. A., Mandelkow, E., Taylor, J. P., & Hyman, B. T. (2018, Apr 3). Tau protein liquid-liquid phase separation can initiate tau aggregation. *EMBO J, 37*(7). https://doi.org/10.15252/embj.201798049

Wippich, F., Bodenmiller, B., Trajkovska, M. G., Wanka, S., Aebersold, R., & Pelkmans, L. (2013, Feb 14). Dual specificity kinase DYRK3 couples stress granule condensation/dissolution to mTORC1 signaling. *Cell, 152*(4), 791-805. https://doi.org/10.1016/j.cell.2013.01.033

Woodruff, J. B., Ferreira Gomes, B., Widlund, P. O., Mahamid, J., Honigmann, A., & Hyman, A. A. (2017, Jun 1). The Centrosome Is a Selective Condensate that Nucleates Microtubules by Concentrating Tubulin. *Cell, 169*(6), 1066-1077 e1010. https://doi.org/10.1016/j.cell.2017.05.028

Woodruff, J. B., Wueseke, O., & Hyman, A. A. (2014, Sep 05). Pericentriolar material structure and dynamics. *Philos Trans R Soc Lond B Biol Sci, 369*(1650). https://doi.org/10.1098/rstb.2013.0459

Woodruff, J. B., Wueseke, O., Viscardi, V., Mahamid, J., Ochoa, S. D., Bunkenborg, J., Widlund, P. O., Pozniakovsky, A., Zanin, E., Bahmanyar, S., Zinke, A., Hong, S. H., Decker, M., Baumeister, W., Andersen, J. S., Oegema, K., & Hyman, A. A. (2015, May 15). Regulated assembly of a supramolecular centrosome scaffold in vitro. *Science, 348*(6236), 808-812. https://doi.org/10.1126/science.aaa3923

Wootton, J. C. (1994, Sep). Non-globular domains in protein sequences: automated segmentation using complexity measures. *Comput Chem, 18*(3), 269-285. https://www.ncbi.nlm.nih.gov/pubmed/7952898

Wueseke, O., Zwicker, D., Schwager, A., Wong, Y. L., Oegema, K., Julicher, F., Hyman, A. A., & Woodruff, J. B. (2016, Oct 15). Polo-like kinase phosphorylation determines Caenorhabditis elegans centrosome size and density by biasing SPD-5 toward an assembly-competent conformation. *Biol Open, 5*(10), 1431-1440. https://doi.org/10.1242/bio.020990

Zeng, M., Shang, Y., Araki, Y., Guo, T., Huganir, R. L., & Zhang, M. (2016, Aug 25). Phase Transition in Postsynaptic Densities Underlies Formation of Synaptic Complexes and Synaptic Plasticity. *Cell, 166*(5), 1163-1175 e1112. https://doi.org/10.1016/j.cell.2016.07.008

Zhang, J. P., Li, X. L., Li, G. H., Chen, W., Arakaki, C., Botimer, G. D., Baylink, D., Zhang, L., Wen, W., Fu, Y. W., Xu, J., Chun, N., Yuan, W., Cheng, T., & Zhang, X. B. (2017, Feb 20). Efficient precise knockin with a double cut HDR donor after CRISPR/Cas9-mediated double-stranded DNA cleavage. *Genome Biol, 18*(1), 35. https://doi.org/10.1186/s13059-017-1164-8

Zhang, Q., Huang, H., Zhang, L., Wu, R., Chung, C. I., Zhang, S. Q., Torra, J., Schepis, A., Coughlin, S. R., Kornberg, T. B., & Shu, X. (2018, Jan 18). Visualizing Dynamics of Cell Signaling In Vivo with a Phase Separation-Based Kinase Reporter. *Mol Cell, 69*(2), 347. https://doi.org/10.1016/j.molcel.2018.01.008

Zheng, Y., Jung, M. K., & Oakley, B. R. (1991, May 31). Gamma-tubulin is present in Drosophila melanogaster and Homo sapiens and is associated with the centrosome. *Cell, 65*(5), 817-823. https://doi.org/10.1016/0092-8674(91)90389-g

Zheng, Y., Wong, M. L., Alberts, B., & Mitchison, T. (1995, Dec 07). Nucleation of microtubule assembly by a gamma-tubulin-containing ring complex. *Nature, 378*(6557), 578-583. https://doi.org/10.1038/378578a0

Zimmerman, W. C., Sillibourne, J., Rosa, J., & Doxsey, S. J. (2004, Aug). Mitosis-specific anchoring of gamma tubulin complexes by pericentrin controls spindle organization and mitotic entry. *Mol Biol Cell, 15*(8), 3642-3657. https://doi.org/10.1091/mbc.E03-11-0796

Zwicker, D., Decker, M., Jaensch, S., Hyman, A. A., & Julicher, F. (2014, Jul 1). Centrosomes are autocatalytic droplets of pericentriolar material organized by centrioles. *Proc Natl Acad Sci U S A, 111*(26), E2636-2645. https://doi.org/10.1073/pnas.1404855111

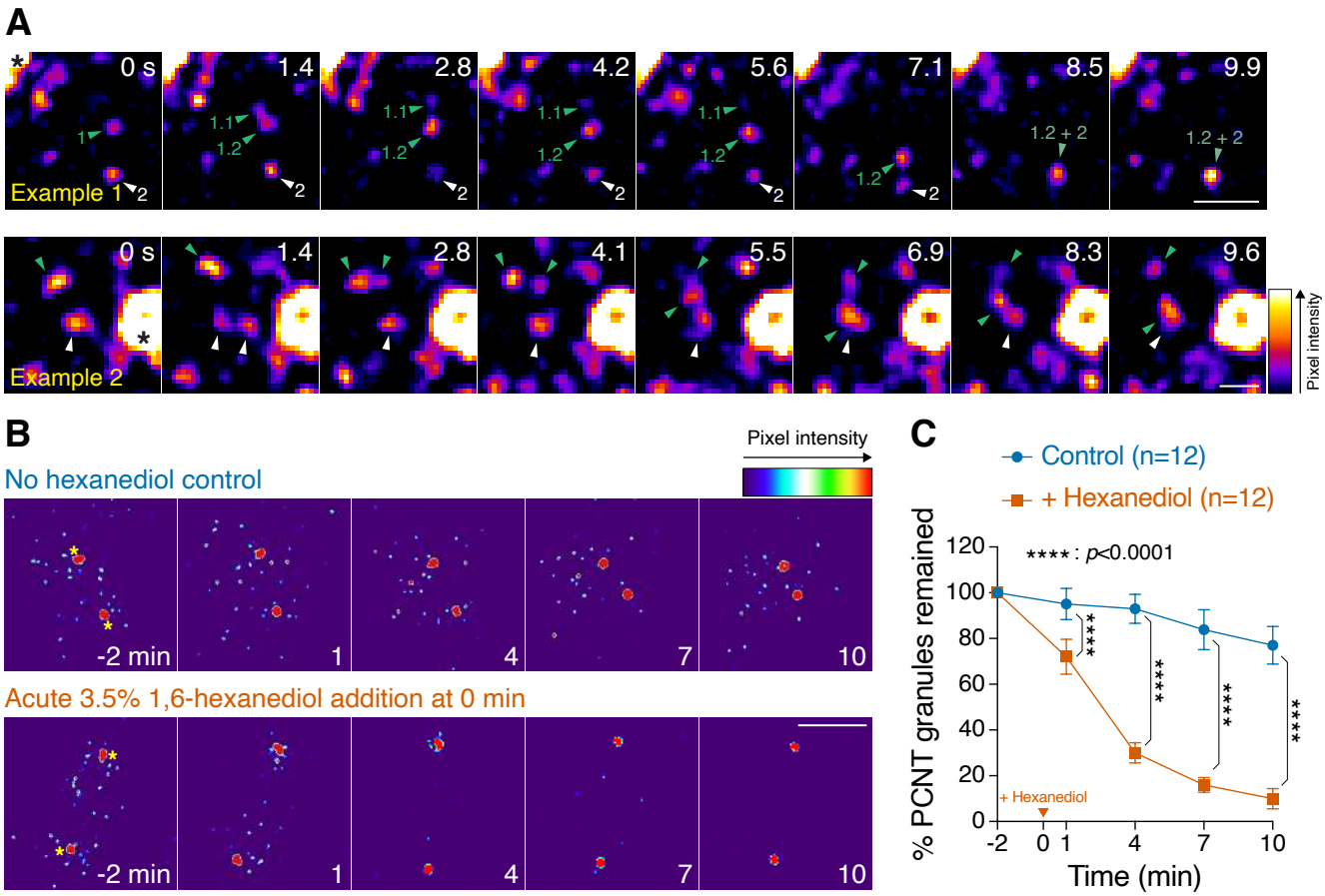

Figure 1. Endogenously expressed GFP-PCNT forms liquid-like condensates during early mitosis. (**A**) Time-lapse micrographs of GFP-PCNT expressed from its endogenous locus during early mitosis. Arrowheads denote the fusing and splitting events of the GFP-PCNT granules. Asterisks in time 0 s denote the centrosomes. The experiment was repeated three times with similar results. (**B**) Time-lapse micrographs of early mitotic cells showing pericentrosomal GFP-PCNT granules without or with the acute 3.5% 1,6-hexanediol treatment. Time 0 is set at the time of hexanediol addition. Asterisks in time -2 min denote the centrosomes. (**C**) Quantification of the results from the experiments shown in (B). Percent of GFP-PCNT granules remained, without and with the acute 1,6-hexanediol treatment, as the function of time was plotted and represented as mean ± 95% CI (confidence intervals) from three biological replicates. The total number of cells analyzed for each condition is indicated. The arrowhead denotes the time of hexanediol addition (time 0). p-values were determined by two-tailed Student's t-test. Scale bars, 1 μm (A, Example 1), 0.5 μm (A, Example 2), and 5 μm (B).

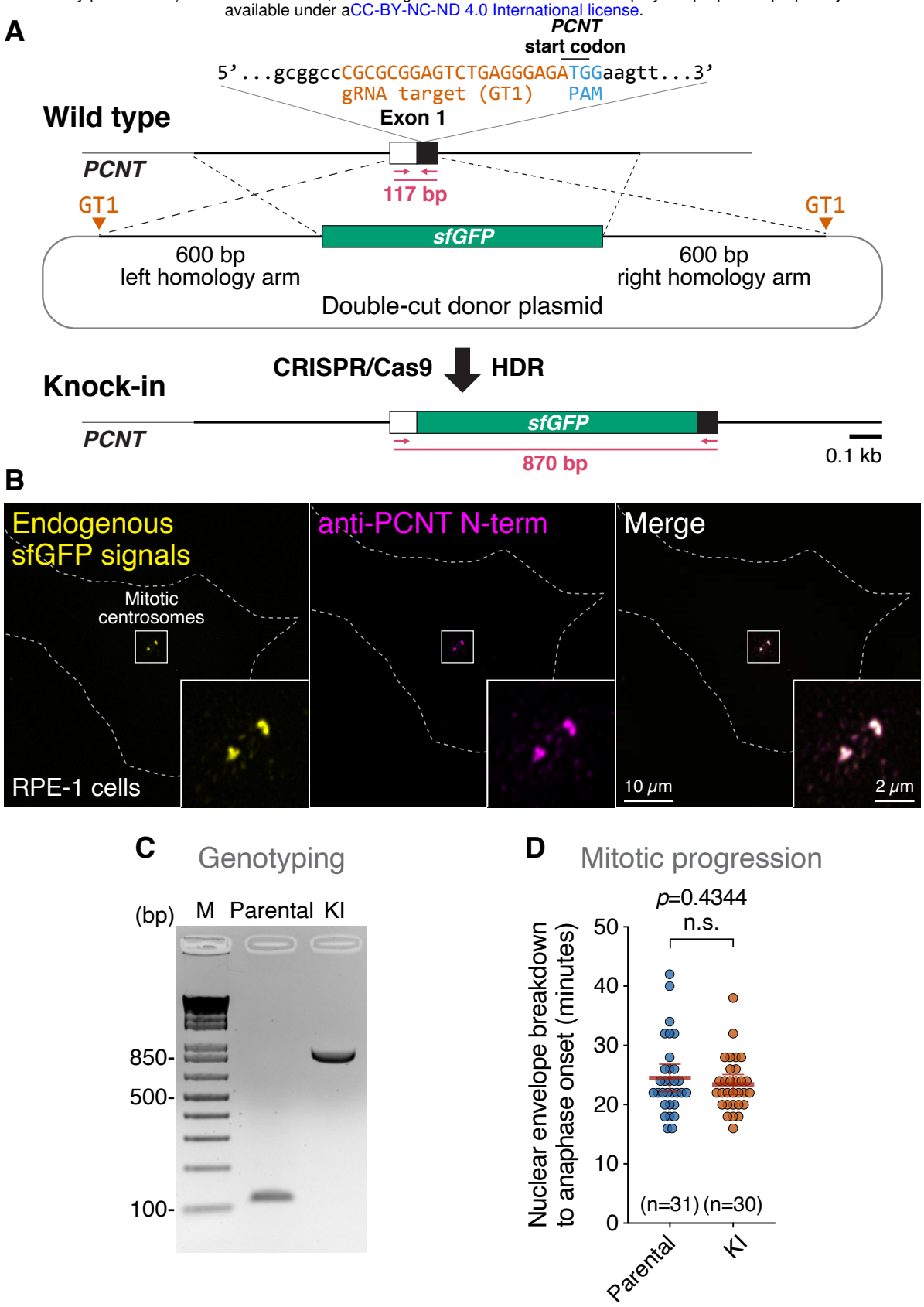

Figure 1- figure supplement 1. Generation and validation of GFP-PCNT knock-in cells. (**A**) Schematic of knocking in *sfGFP* into the *PCNT* locus of RPE-1 cells using the CRISPR/Cas9 technology with a double-cut homology-directed repair (HDR) donor. Arrows indicate the locations of genotyping primers. (**B**) Immunofluorescence images of GFP-PCNT knock-in (KI) cells. The experiment was repeated three times with similar results. (**C**) Genotyping results of the GFP-PCNT KI and the parental cells by polymerase chain reaction (PCR) using the primers indicated in (A). The experiment was repeated three times with similar results. (**D**) Quantification of mitotic durations of GFP-PCNT KI and parental cells stably expressing miRFP670-CETN2 and mScarlet-i-H2A that mark the centrosome and DNA, respectively. Data are mean ± 95% CI. The p-value was determined by two-tailed Student's t-test; n.s., not significant. n, number of cells analyzed from three biological replicates.

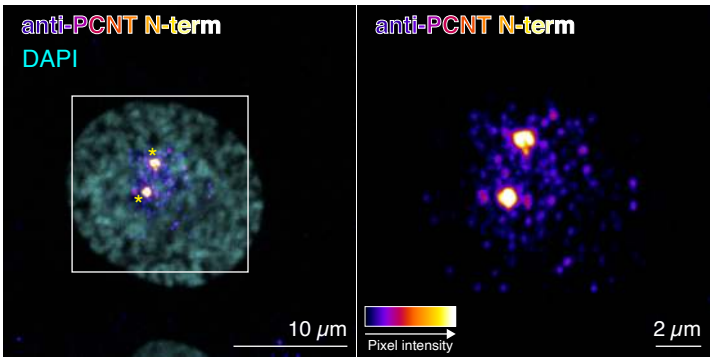

Figure 1- figure supplement 2. PCNT granules near centrosomes during early mitosis. Immunofluorescence of a prophase RPE-1 cell using the anti-PCNT N-terminus antibody to detect endogenous PCNT proteins. Asterisks denote the centrosomes. The experiment was repeated three times with similar results.

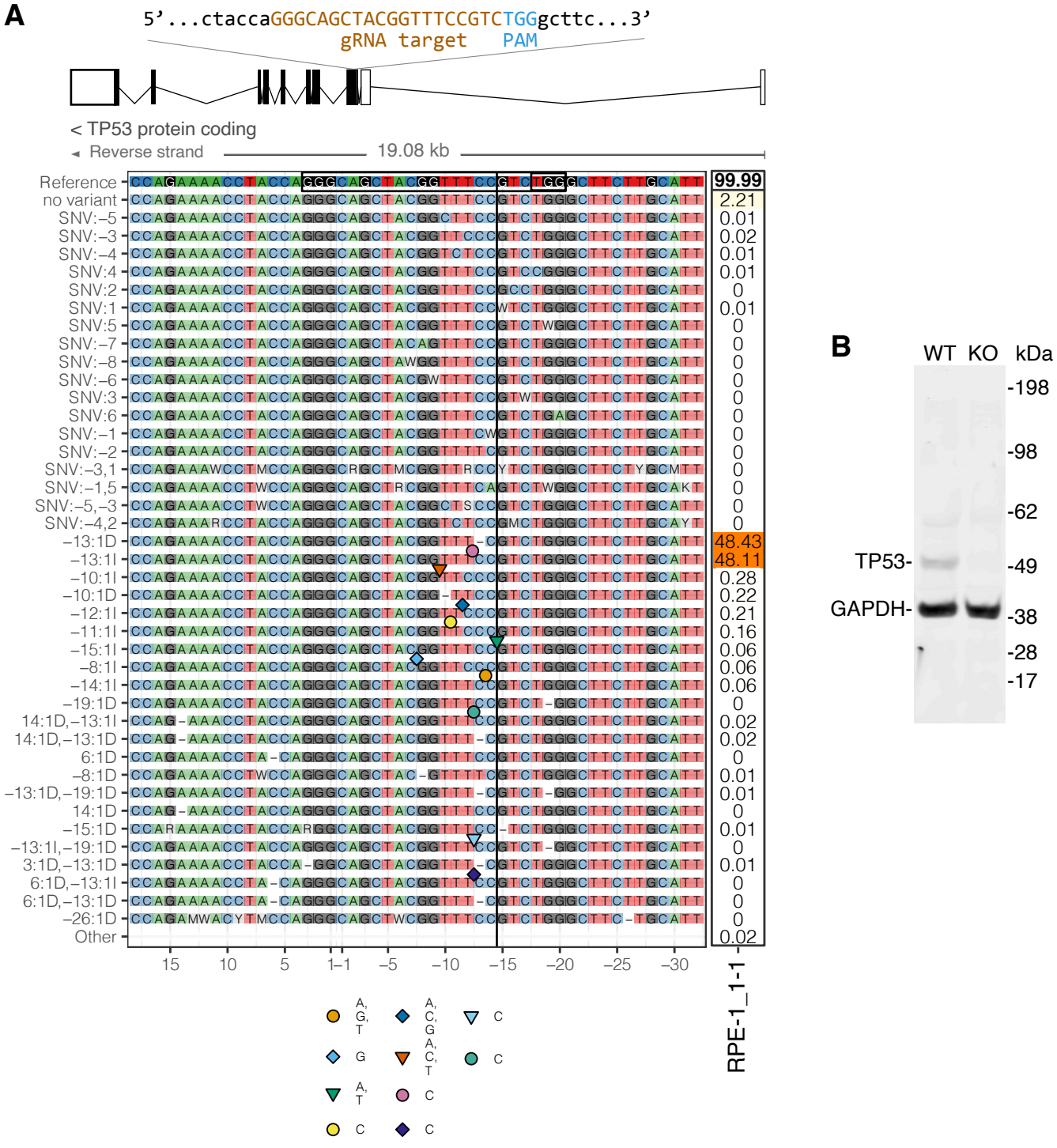

Figure 1- figure supplement 3. Generation of *TP53* knockout RPE-1 cells. (**A**) Illumina sequencing confirmed that one of the CRISPR-edited RPE-1 cell lines, RPE-1_1-1, has frameshift mutations at the gRNA target site in both *TP53* alleles (a 1-bp deletion and a 1-bp insertion). Sequencing data were analyzed and illustrated by an R-based toolkit, CrispRVariants (Lindsay et al., 2016). (**B**) Western blot analysis confirmed the loss of TP53 protein in RPE-1_1-1 cells. Anti-GAPDH staining served as the loading control. WT: parental RPE-1 cells; KO: RPE-1_1-1 cells.

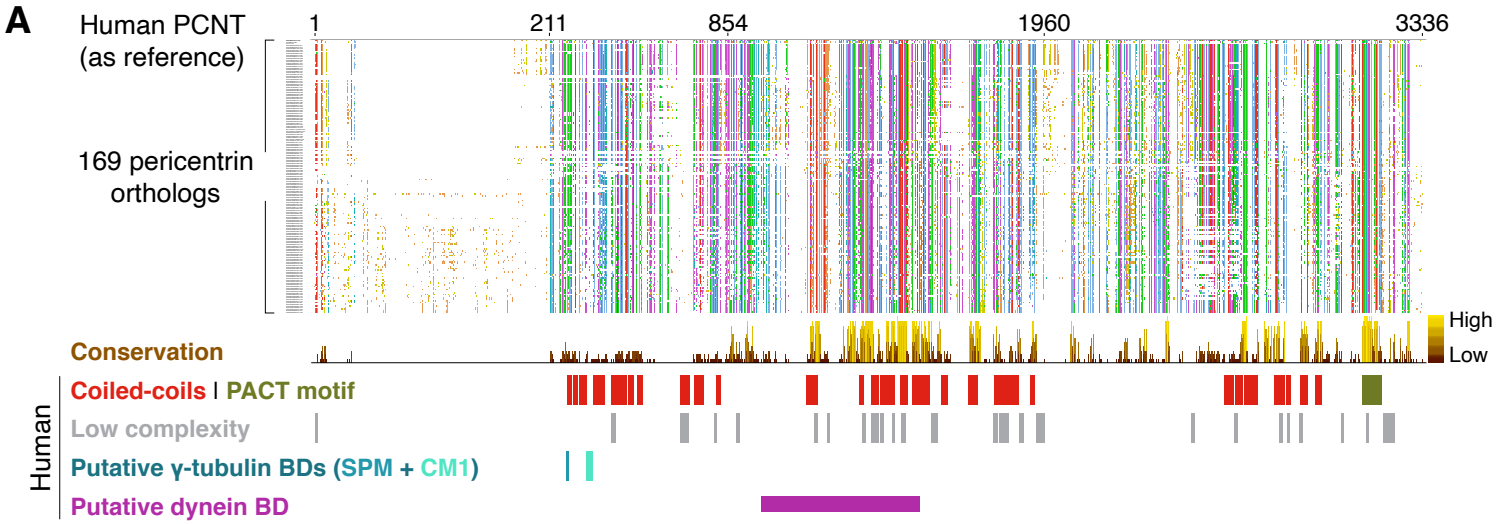

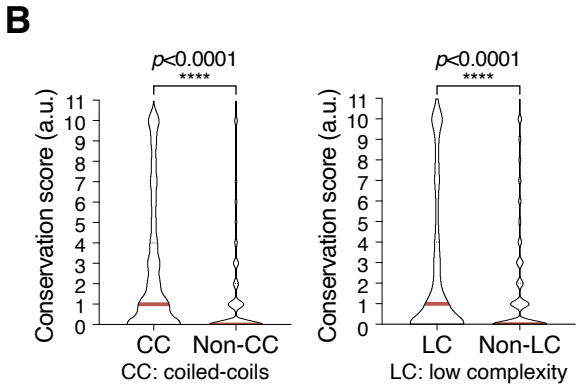

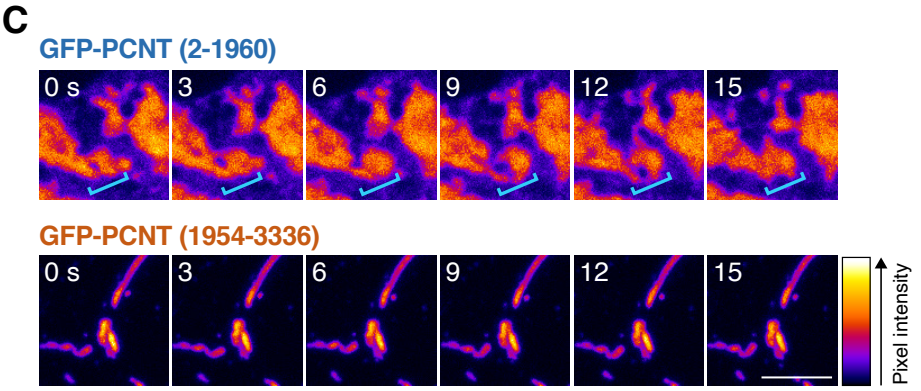

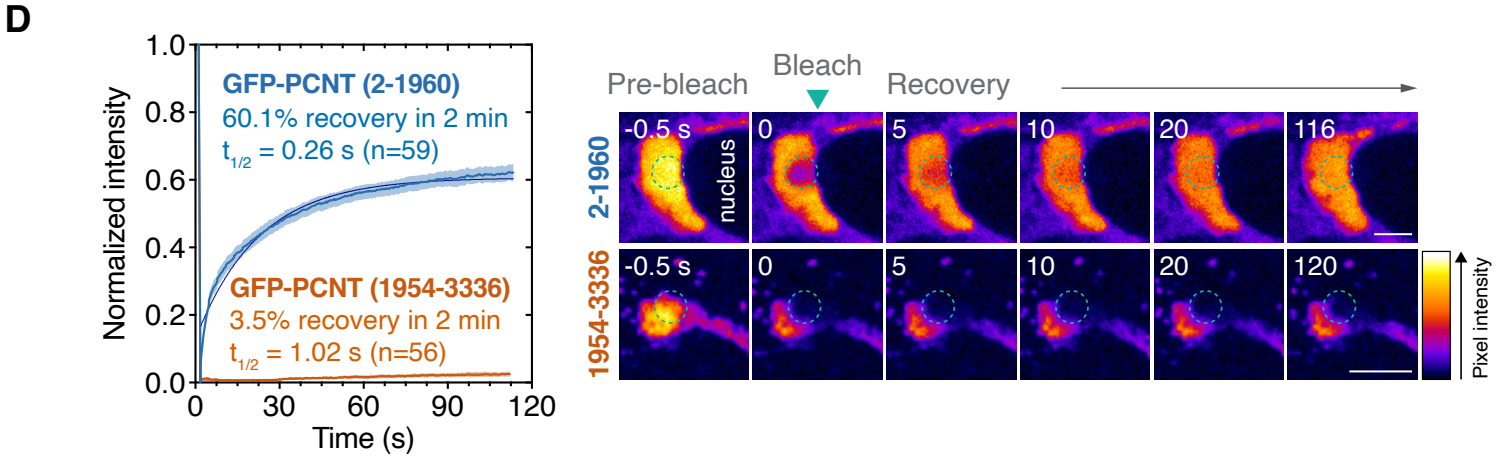

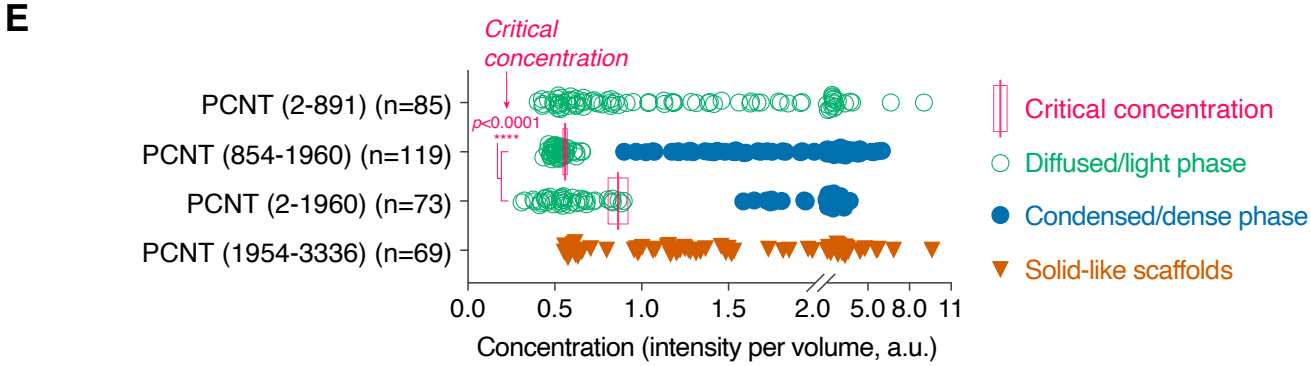

Figure 2. Coiled-coil/LCR-rich N-terminal and middle segments of PCNT phase separate in a concentration-dependent manner. (**A**) An alignment of 169 pericentrin orthologous proteins from vertebrates (167), fruit fly (1), and budding yeast (1) with the conservation scores shown below the alignment. The alignment was colored by the default Clustal X coloring scheme (Figure 2- table 1). Locations of predicted coiled-coils, PACT motif, low-complexity regions, and putative γ-tubulin and dynein binding domains (BDs) of human PCNT are noted below the alignment. (**B**) Distribution of conservation scores corresponding to human PCNT within or outside of the coiled-coil (CC) or low complexity (LC) regions. Data are presented in violin plots, with red bars and dashed lines denoting the median and third quartile, respectively. (**C**) Representative time-lapse micrographs of GFP-tagged PCNT (2-1960) and PCNT (854-1960) 24 h post Dox induction in RPE-1 cells. Brackets denote the dynamic rearrangement of GFP-PCNT (2-1960) condensates. Similar results were observed in three biological replicates. (**D**) FRAP analyses of GFP-PCNT (2-1960) condensates and GFP-PCNT (1954-3336) scaffolds in RPE-1 cells. Dashed circles delineate the bleached sites. Data are mean ± 95% CI. n, number of condensates/scaffolds analyzed from >3 biological replicates. The percent recovery and half-life ($t_{1/2}$) after photobleaching were calculated after fitting the data with non-linear regression. (**E**) Quantification of relative protein concentrations (intensity sum per volume) in live cells expressing various GFP-tagged PCNT segments after Dox induction. Critical concentrations are mean ± 95% CI. n, number of cells analyzed from three biological replicates per segment. The p-values were determined by two-tailed Student's t-test. a.u., arbitrary unit. Scale bars, 5 μm.

Category	Color	Residue at position	{Threshold, Residue group}
Hydrophobic	BLUE	A, I, L, M, F, W, V	{>60%, WLVIMAFCHP}
		C	{>60%, WLVIMAFCHP}
Positive charge	RED	K, R	{>60%, KR}, {>80%, K, R, Q}
Negative charge	MAGENTA	E	{>60%, KR}, {>50%, QE}, {>85%, E, Q, D}
		D	{>60%, KR}, {>85%, K, R, Q}, {>50%, ED}
Polar	GREEN	N	{>50%, N}, {>85%, N,Y}
		Q	{>60%, KR}, {>50%, QE}, {>85%, Q, E, K, R}
		S, T	{>60%, WLVIMAFCHP}, {>50%, TS}, {>85%, S, T}
Cysteines	PINK	C	{>85%, C}
Glycines	ORANGE	G	{>0%, G}
Prolines	YELLOW	P	{>0%, P}
Aromatic	CYAN	H, Y	{>60%, WLVIMAFCHP}, {>85%, W, Y, A, C, P, Q, F, H, I, L, M, V}
Unconserved	WHITE	any/gap	If none of the above criteria are met

Figure 2- table 1. Clustal X coloring scheme (adapted from Jalview) used in the multi-species alignment in Figure 2A.

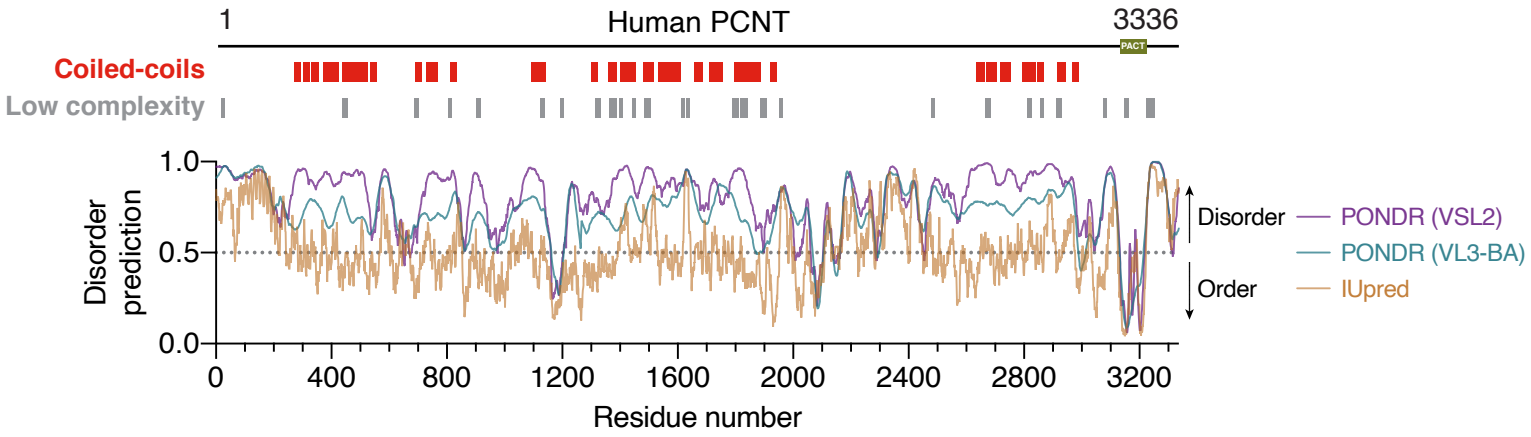

Figure 2- figure supplement 1. Disorder predictions of human PCNT. Predicted coiled-coils and low-complexity regions of human PCNT aligned with results of three disorder prediction algorithms (PONDR VSL2, PONDR VL3-BA, and IUpred).

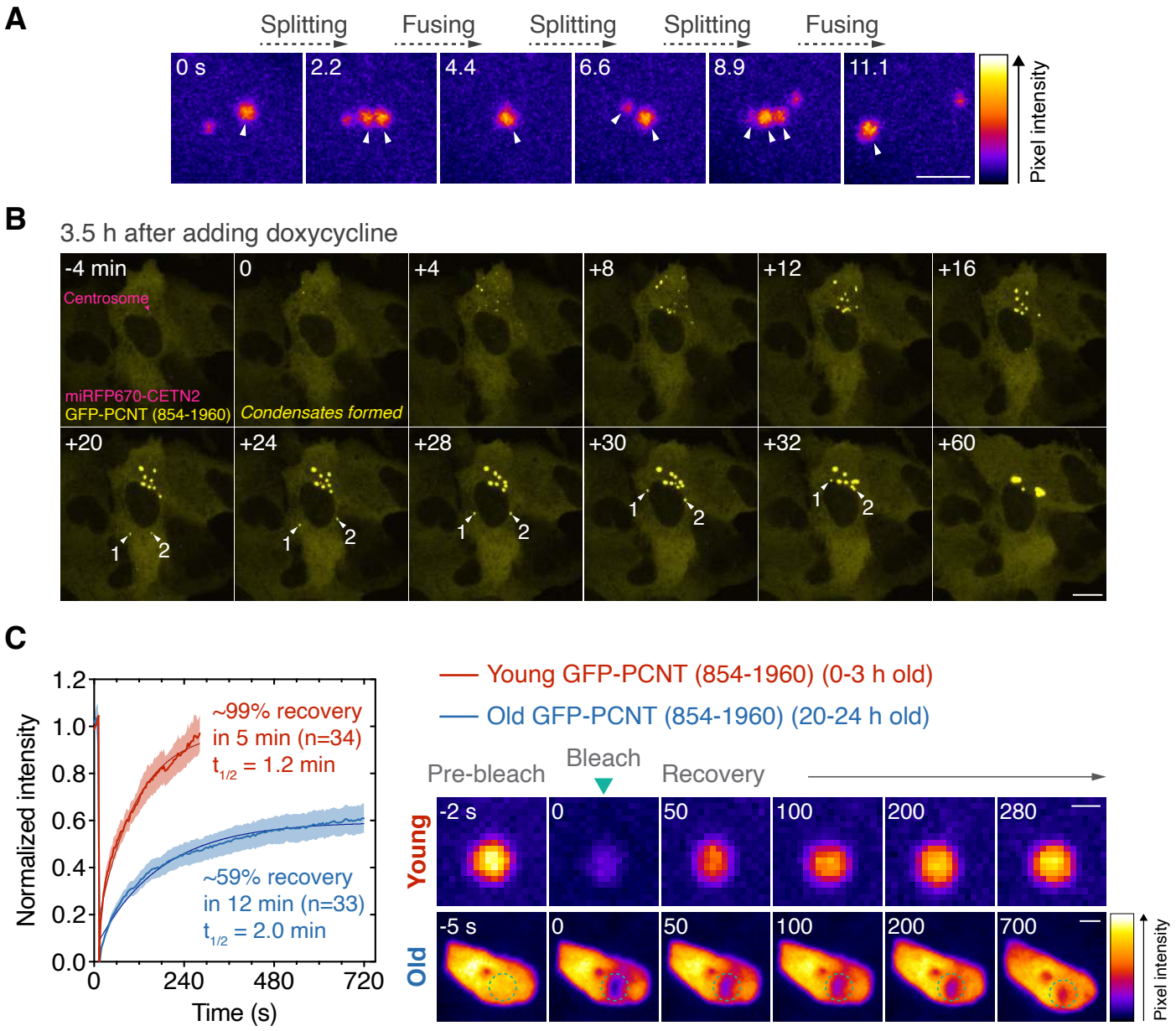

Figure 3. GFP-PCNT (854-1960) undergoes liquid-liquid phase separation, coalesces, and moves toward the centrosome. (**A**) Time-lapse micrographs of GFP-PCNT (854-1960) condensates in RPE-1 cells. Arrowheads denote the fast fusing and splitting events of the spherical condensates. Similar results were observed in three biological replicates. (**B**) Time-lapse micrographs of GFP-PCNT (854-1960) expressed in miRFP670-CETN2-positive RPE-1 cells. Time-lapse imaging started 3.5 h post Dox induction. The time when the first condensates formed is marked as time 0. Arrowheads denote the examples of two condensates moving around the nucleus toward the centrosome. The experiment was repeated more than three times with similar results. (**C**) FRAP analysis of different ages of GFP-PCNT (854-1960) condensates in RPE-1 cells. Dashed circles delineate the bleached sites. Data are mean ± CI. n, number of condensates analyzed from three biological replicates. The percent recovery and half-life ($t_{1/2}$) after photobleaching were calculated after fitting the data with non-linear regression. Note that the highly mobile nature of young condensates prevented us from tracking the same condensates consistently beyond 5 min in the recovery phase of the FRAP assay. Scale bars, 2 μm (A), 10 μm (B), 1 μm (C, young condensates), and 2 μm (C, old condensates).

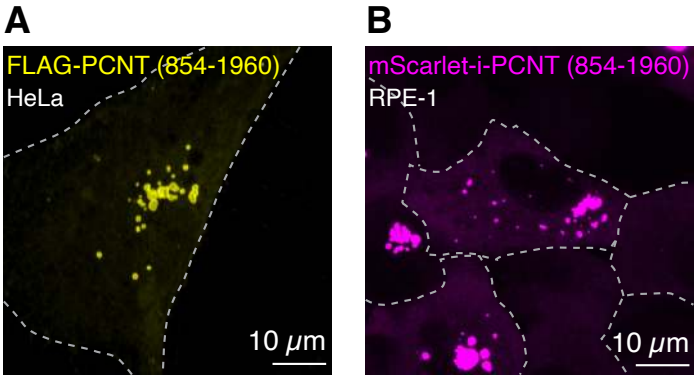

Figure 3- figure supplement 1. FLAG- and mScarlet-i-tagged PCNT (854-1960) fusion proteins form condensates. (**A**) Anti-PCNT N-terminus immunofluorescence of HeLa cells transiently expressing FLAG-PCNT (854-1960). The experiment was repeated two times with similar results. (**B**) mScarlet-i-PCNT (854-1960) condensates in live RPE-1 cells. Dashed lines delineate the cell boundaries. The experiment was repeated three times with similar results.

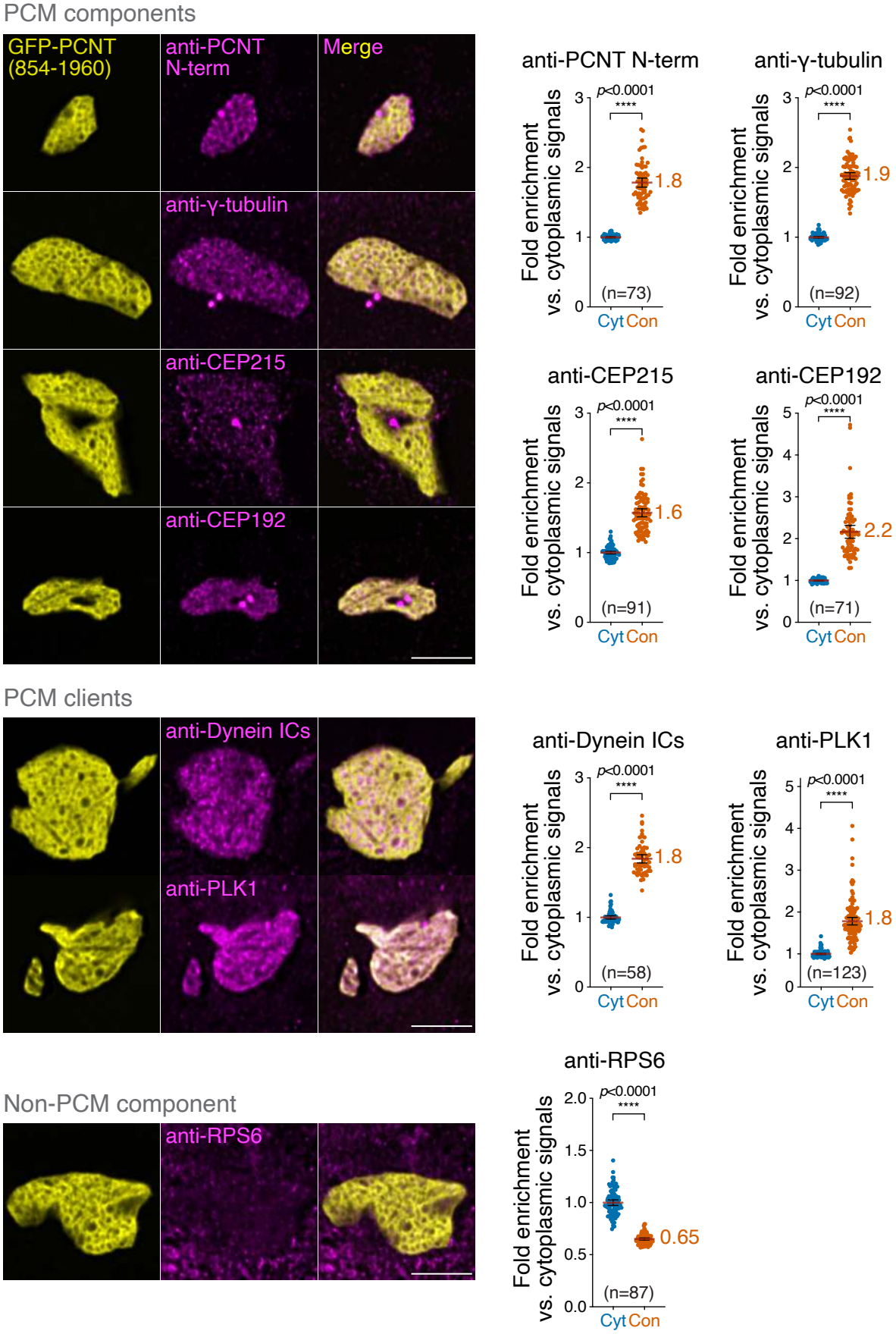

Figure 4. GFP-PCNT (854-1960) condensates selectively recruit endogenous PCM components. Immunofluorescence of PCNT N-terminus (PCNT N-term), γ-tubulin, CEP215, CEP192, cytoplasmic dynein intermediate chains (Dynein ICs), PLK1, or ribosomal protein S6 (RPS6) in RPE-1 cells after Dox induction to form GFP-PCNT (854-1960) condensates. Fold enrichment of fluorescence signals in the condensate (Con) relative to those in the cytoplasm (Cyt) was quantified. Data are mean ± 95% CI. Fold enrichment mean values are noted. n, number of cells analyzed from at least two biological replicates per protein. p-values were determined by two-tailed Student's t-test. Scale bars, 5 μm.

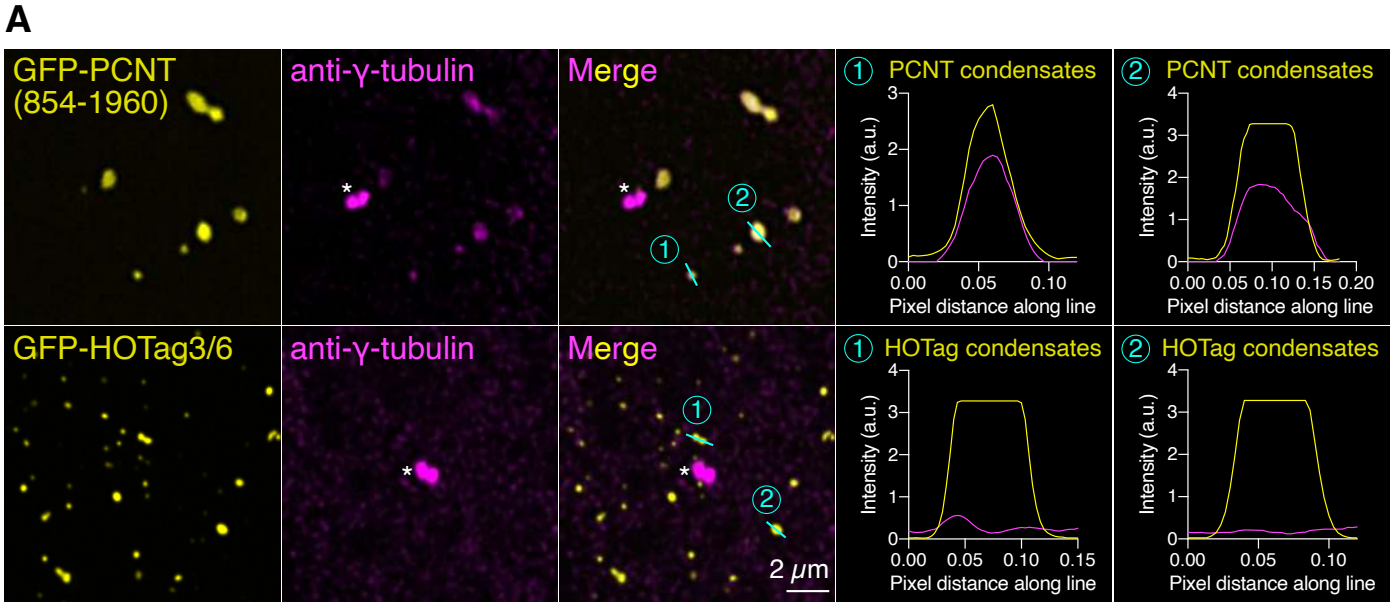

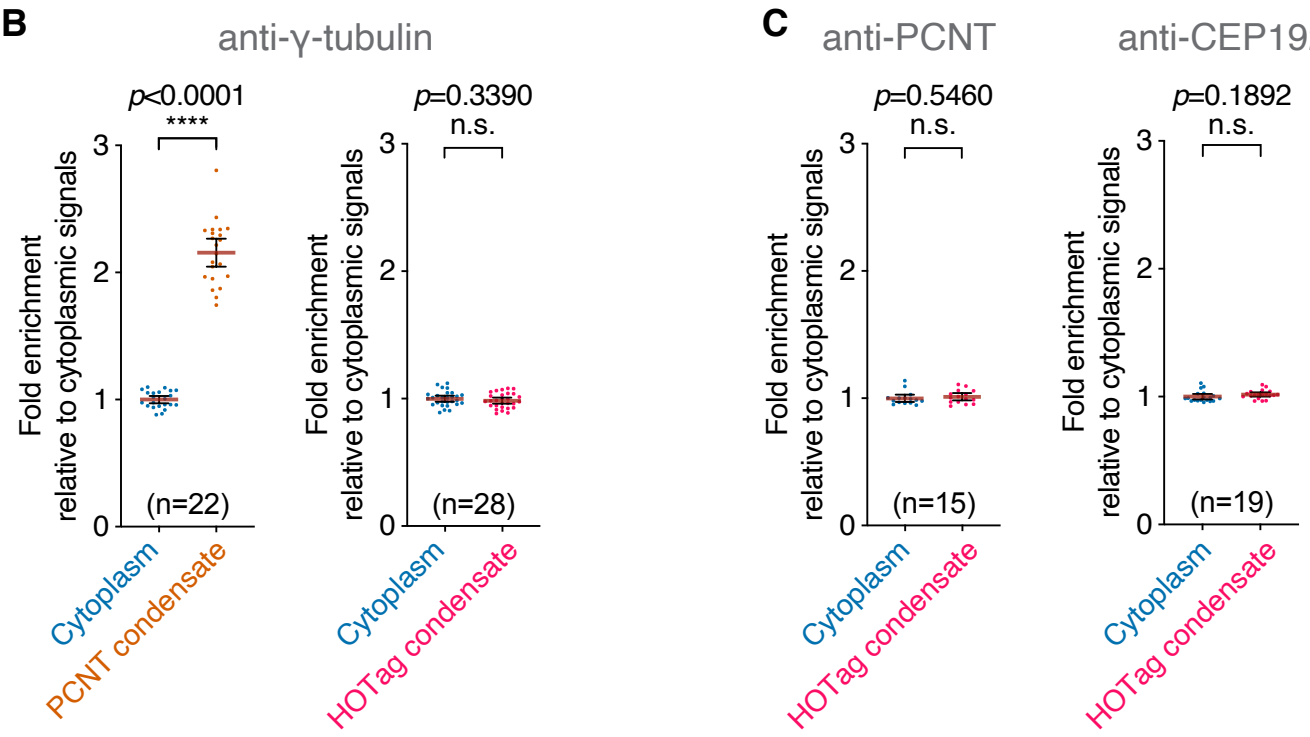

Figure 4- figure supplement 1. Endogenous PCM components are not enriched in the HOTag condensates. (**A**) Anti-γ-tubulin immunofluorescence of GFP-PCNT (854-1960) and GFP-HOTag3/6 condensates. Right: The line plots of the selected regions (cyan lines). Asterisks denote the centrosomes. (**B** and **C**) Fold enrichment of fluorescence signals in the PCNT or HOTag condensates relative to those in the cytoplasm was quantified. Data are mean ± 95% CI. p-values were determined by two-tailed Student's t-test. n.s., not significant. n, number of cells analyzed from two, one, and two biological replicates for γ-tubulin, PCNT, and CEP192, respectively.

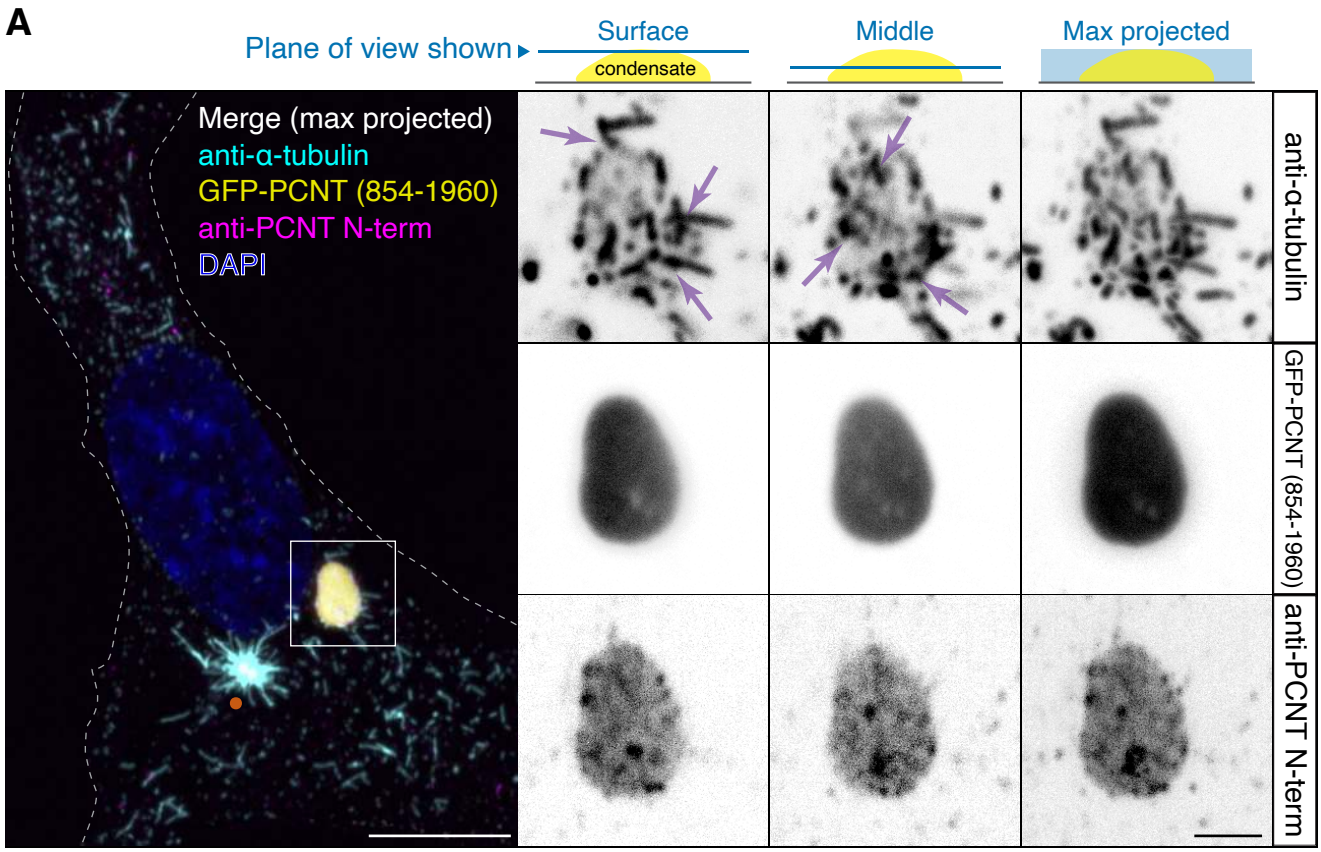

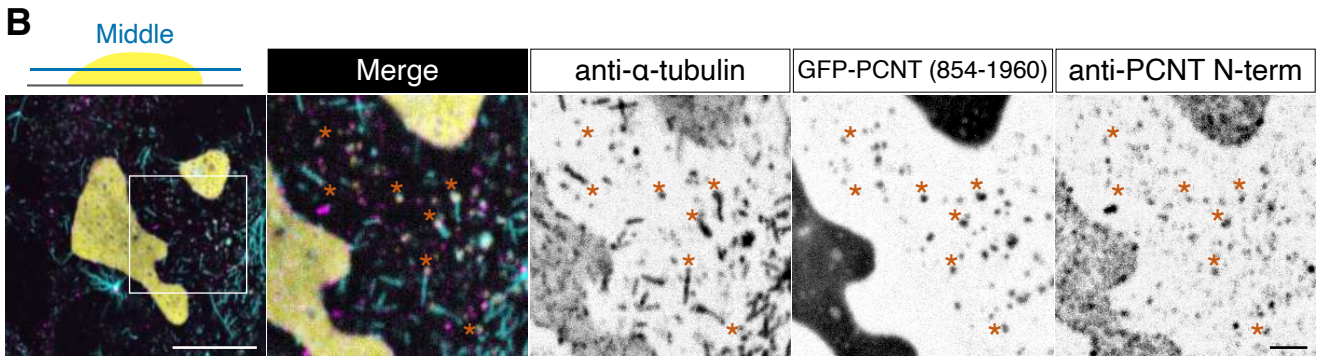

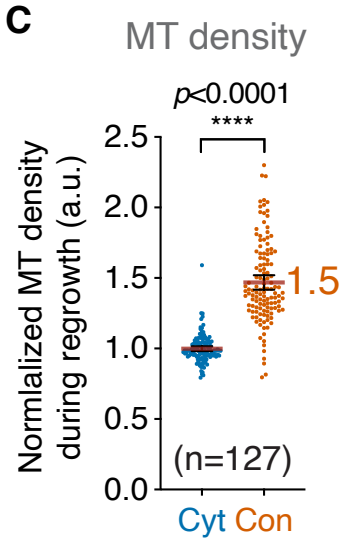

Figure 5. GFP-PCNT (854-1960) condensates nucleate MTs in cells. (**A**) Anti-α-tubulin immunofluorescence of GFP-PCNT (854-1960) condensates during MT renucleation in max-projected and single optical section views. Note that MTs were renucleated within and on the surface of the condensate (arrows). A dot in the merged channels denotes the centrosome, where MT renucleation was robust. (**B**) MT renucleation also occurred in small PCNT condensates (asterisks), which also recruited endogenous PCNT. (**C**) Quantification of MT density in GFP-PCNT (854-1960) condensates (Con) and in the surrounding cytoplasm (Cyt) during MT renucleation. Data are mean ± 95% CI. Fold enrichment mean value is noted. n, number of condensates analyzed from three biological replicates. The p-value was determined by two-tailed Student's t-test. a.u., arbitrary unit. Scale bars, 10 μm and 2 μm (inset).

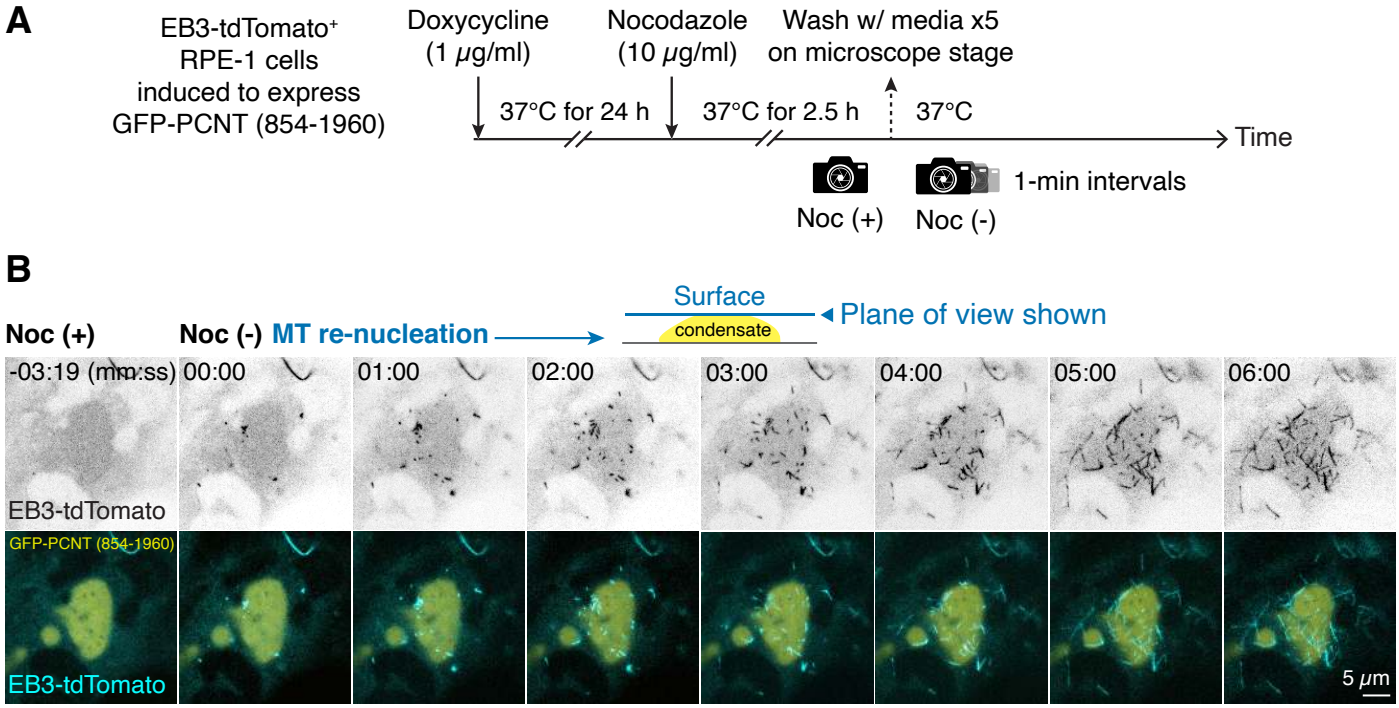

Figure 5- figure supplement 1. GFP-PCNT (854-1960) condensates nucleate MTs in live cells. (**A**) Schematic of the MT renucleation assay in live cells. GFP-PCNT (854-1960) condensates in EB3-tdTomato-positive RPE-1 cells were formed after Dox induction. MTs were then depolymerized by nocodazole (Noc). A pre-wash image was taken [Noc (+)], followed by time-lapse imaging at 1-min intervals after nocodazole was washed out on the microscope stage to follow MT renucleation [Noc (-)]. (**B**) Single optical sections of time-lapse micrographs of EB3-tdTomato-labeled microtubule plus ends on the surface of a GFP-PCNT (854-1960) condensate during MT renucleation. Time 0 was the time immediately after nocodazole was washed out. The experiment was repeated three times with similar results.

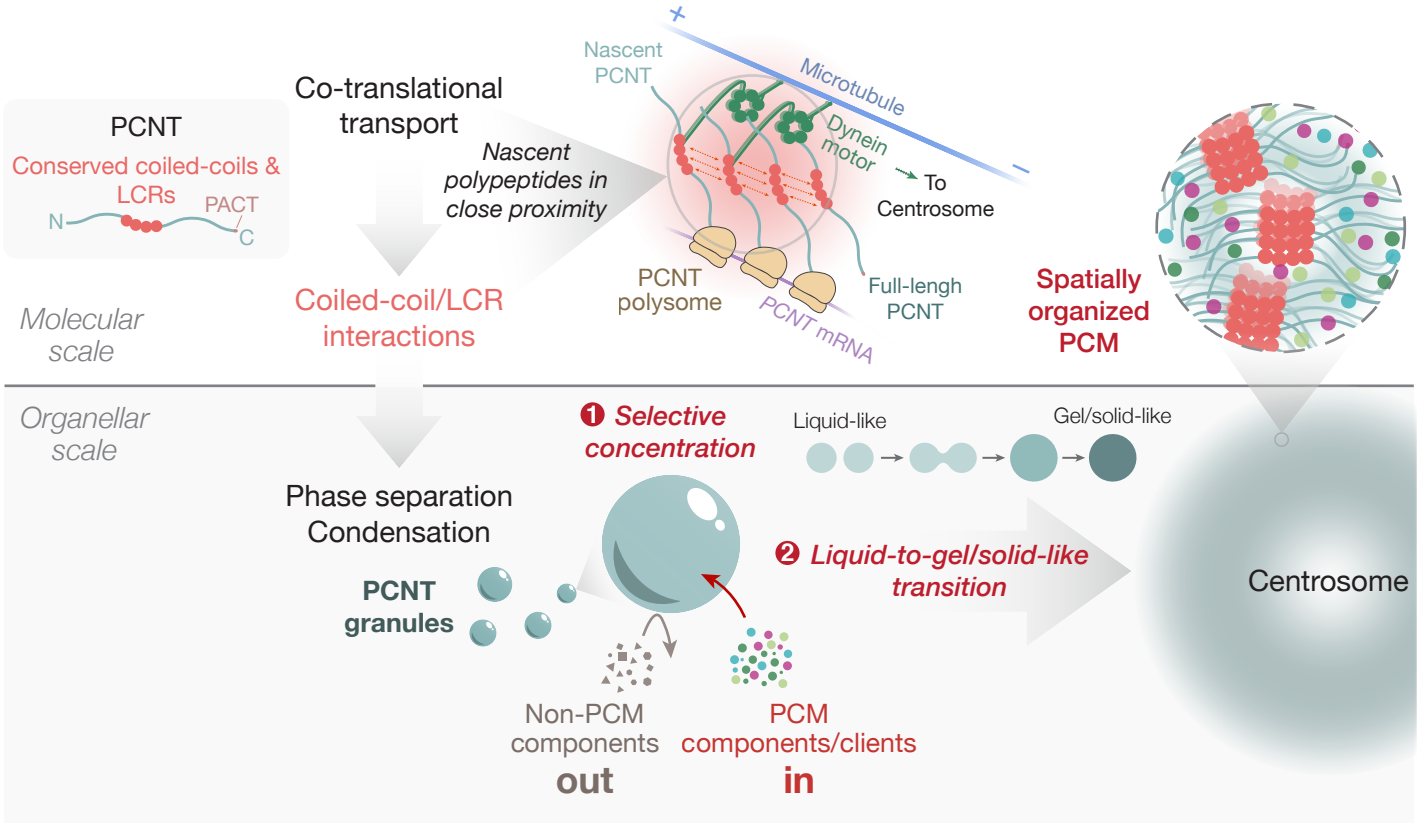

Figure 6. Model for PCNT phase separation in centrosome assembly. PCNT is a linear multivalent protein that phase separates through its conserved coiled-coils and LCRs during its co-translational targeting to the centrosome when the nascent PCNT polypeptides are in close proximity in the polysome. The resulting PCNT granules/condensates promote PCM assembly by (1) selectively concentrating PCM components and clients; this will facilitate and limit the biochemical reactions that eventually take place at the centrosome (e.g., MT nucleation, kinase activities) and (2) enabling a liquid-to-gel/solid-like transitioning process during centrosome assembly; this process provides the PCM components a thermodynamically favored pathway to assemble into a micron-sized, membraneless, and yet spatially organized PCM.